NTNU – Trondheim
Norwegian University of
Science and Technology

Sensitivity of seismic well ties to attenuation effects

Marcelina Karen
Czajkowski

Petroleum Geoscience and Engineering
Submission date: June 2015
Supervisor: Ketil Hokstad, IPT
Co-supervisor: Andrew James Carter, Statoil ASA

Norwegian University of Science and Technology
Department of Petroleum Engineering and Applied Geophysics

Abstract

Seismic attenuation affects seismic data by reducing the amplitudes, by imposing phase distortion and by decreasing the data bandwidth. These effects need to be adequately managed to obtain satisfactory well ties. In this study two experiments were performed to assess the detectability of phase Q effects on seismic well ties. The effects were to be quantitatively determined by studying the wavelets extracted from well ties. The first experiment was carried out to study the attenuation effects on synthetic data, to establish whether the software was adequate for wavelet extractions, and to obtain a set of parameters with which to perform wavelet extractions. The second experiment was then performed to assess the detectability of phase Q effects using data from a real seismic survey. Wavelets were extracted from two seismic well tie windows to check the stability of the wavelets with time. The synthetic experiment successfully extracted wavelets and was deemed suitable for wavelet extractions. Attenuation effects were evident from the wavelets. The wavelets estimated from the second experiment also showed the effects of Q. Both experiments implied that the outcome of imposing a time shift on a wavelet was equivalent to a wavelet of the same shape estimated using a different reference frequency for Q modeling.

Sammendrag

Seismisk dempning påvirker seismiske data ved å redusere amplitudene, ved å innføre faseforvrengning og ved å redusere databåndbredden. Disse effektene må være tilstrekkelig håndtert for å oppnå tilfredsstillende brønntie. I denne studien ble to eksperimenter utført for å vurdere hvorvidt fase Q effekter var tydelige fra seismiske brønntie. Effektene skulle bestemmes kvantitativt ved å studere wavelets ekstrahert fra brønntie. Det første ekperimentet ble utført for å studere dempingseffekter på syntetiske data, for å etablere hvorvidt programvaren var tilstrekkelig for wavelet ekstraksjoner, og for å oppnå et sett parametere med hvilke man kunne estimere wavelet. Det andre forsøket ble deretter utført for å vurdere om fase Q effekter var tydelige ved bruk av data fra en ekte seismisk undersøkelse. Wavelets ble ekstrahert fra to seismiske brønntie vinduer for å kontrollere stabiliteten av waveletene med tid. Det syntetiske eksperimentet var vellykket med å uthente wavelets. Dempingseffektene var tydelige fra waveletene. Wavelets estimert fra det andre eksperimentet viste også virkninger av Q. Begge forsøkene antydet at resultatet av å innføre en tidsforskyvning på en wavelet var ekvivalent med en wavelet av samme form estimert ved hjelp av en annen referansefrekvens for Q modellering.

Preface

This project was performed as a collaboration between the Norwegian University of Science an Technology and Statoil ASA. I would like to acknowledge my supervisors Prof. II Ketil Hokstad and Dr. Andrew James Carter, and thank for their help and support that was given me. I would also like to thank other colleagues at Statoil for valuable input.

Contents

List of Figures

List of Tables

1

Introduction

The results obtained from seismic well ties are useful for several geophysical applications such as seismic interpretation, amplitude versus offset (AVO) modeling, seismic inversion, to name a few. Seismic attenuation however affects seismic data by reducing the amplitudes, by imposing velocity dispersion on the frequency components thus distorting the phase of the components, and by reducing the data bandwidth. All of these effects need to be properly handled to obtain satisfactory well ties. A question then arises as to whether the effects of seismic attenuation are evident from seismic well ties. Can the effects of attenuation be quantitatively determined by for instance studying the wavelet with which a seismic well tie is performed? What would the significance of these effects be?

In this study two experiments were carried out with the intention of assessing the detectability of phase attenuation effects on seismic well ties. An experiment was first performed to assess the detectability using synthetic data. The experiment was also carried out to test whether the well tie software was suitable for wavelet extractions using a specific method as proposed by White (1980). Furthermore, a set of parameters with which to perform wavelet extractions was to be established. A second experiment was then carried out to assess if effects were detectable from a well tie using data from a real seismic survey at Åsgard.

2

Geological setting

The Halten Terrace is located on the mid-Norwegian continental shelf approximately 200 km off the coast of Norway between 64° and 65°30'N, and between 6° and 8°E. The Statoil operated Åsgard field is situated on the Halten Terrace and includes the discoveries Midgard, Smørbukk and Smørbukk Sør discovered in 1981, 1984, and 1985 respectively (see Figure 2.1). This study has been carried out using data from Smørbukk Sør, which is located in licence block 6506/12 with part of it expanding into block 6406/3 in the south. Smørbukk Sør was discovered by well 6506/12-3 with currently producing reservoirs at approximately 3800-4200 m below sea level. However, hydrocarbons have also been encountered at shallower depths around 3100 m, named the Blåbjørn discovery (Zaki et al., 2011).

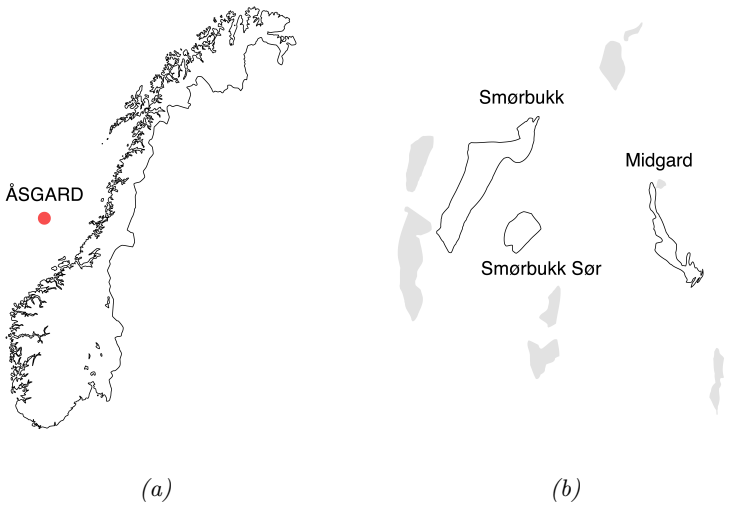

Figure 2.1: (a) Location of Åsgard relative to Norway. (b) Outlines of Midgard, Smørbukk, Smørbukk Sør and neighboring fields in grey.

The mid-Norwegian continental margin has a complex tectonic history distinguished by crustal extension that initiated during the Devonian. Rift basins continued to develop throughout the Triassic with predominant deposition of continental clastics and evaporites. Subsequently a shallow seaway formed in the rift area in the Early Jurassic. Thick coal beds were deposited on coastal plains and overlain by deltaic to shallow marine sediments, which were strongly influenced by a fluctuating coastline (Bøe et al., 2010). The depositional environment became increasingly more open-marine throughout the Middle Jurassic.

A major rifting episode initiated in the Middle Jurassic and lasted into the Early Cretaceous establishing numerous rotated fault blocks and faults that soled out into the Triassic evaporites (Bell et al., 2014). During this time deposition of organic-rich mud also occurred. In the Cretaceous deep marine sediments were deposited, and another rifting episode followed leading to the continental separation of Greenland and Eurasia. Active seafloor spreading thus commenced in the Early Eocene resulting in the formation of deep, regional basins filled with clastic sediments that had been carried from the continental areas (Bøe et al., 2010). Seafloor spreading is still continuing at the present day.

Smørbukk Sør is located on the crest of a dome-like structure that forms a four-way dip closure. The structure is bounded by major faults to the east and west, and likely developed during the Late Jurassic due to a combination of salt doming and extensional faulting (Martinius et al., 2005). Hydrocarbons originate from two types of source rocks; coals that are gas and condensate-prone in the Early Jurassic Åre Formation, and shales that are oil-prone in the Late Jurassic Spekk Formation. The reservoirs are the mudstone-dominated sediments of the Early Jurassic Tilje Formation and the well-sorted sandstones of the Middle Jurassic Ile and Garn Formations (Koch & Heum, 1995).

The primary reservoir quality of the Ile and Garn Formations is excellent, however it decreases with depth as a result of quartz cementation and illitization. The Tilje Formation, on the other hand, has variable reservoir quality due to its heterolithic nature, but chlorite coating of grains has preserved good reservoir properties even at greater depths. Additionally, an accumulation of hydrocarbons has been discovered in the turbiditic sandstones of the Late Cretaceous Lysing Formation (Koch & Heum, 1995). Overlying mudstones act as seals for the reservoirs, as can be seen from the stratigraphic column (Figure 2.2).

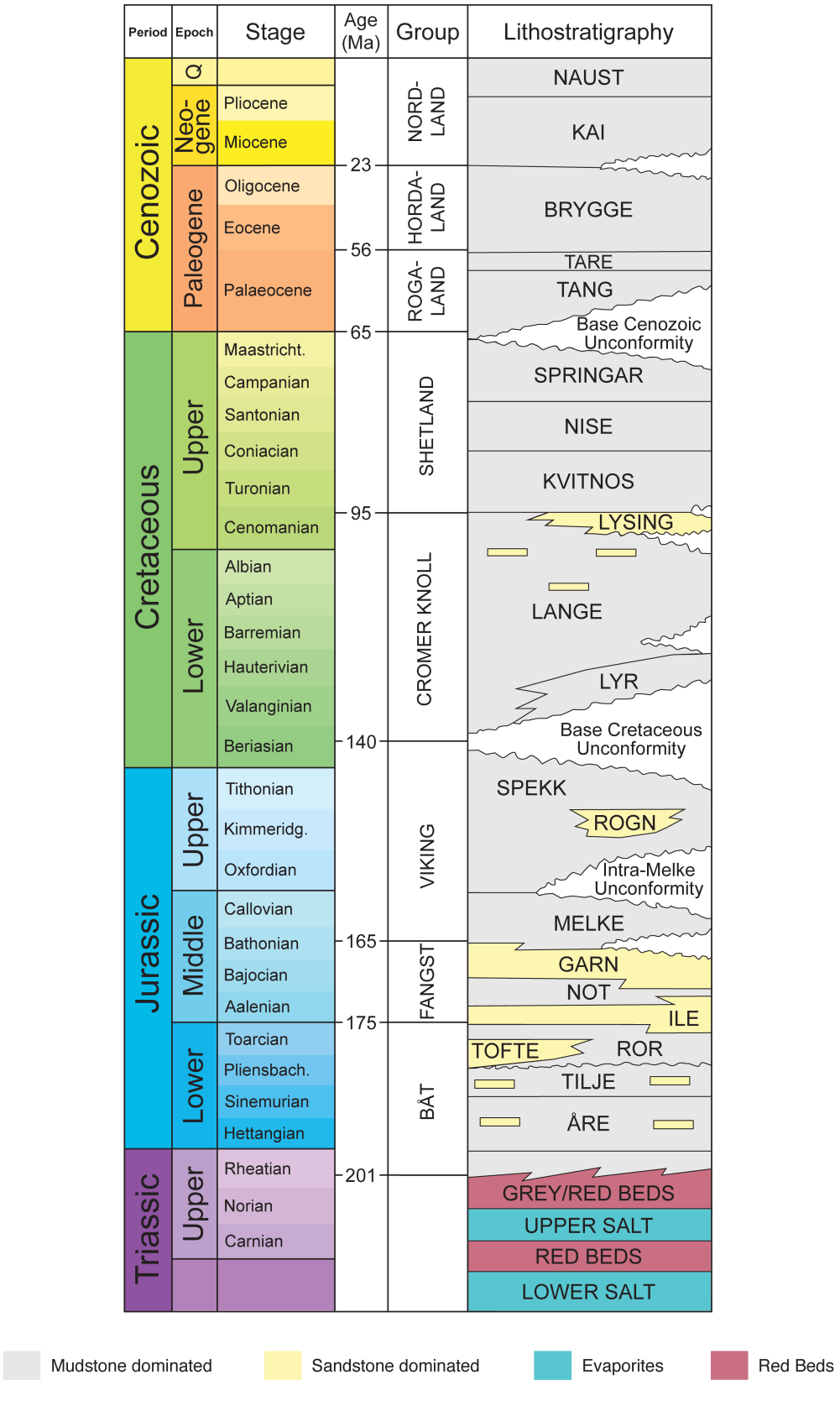

Figure 2.2: Stratigraphic column over the Halten Terrace, after Bell et al. (2014).

3

Theoretical Background

3.1 Understanding the wavelet

For the purposes of tying seismic time sections to geology at wells the seismic reflection signal can often be described by a simple model. In this model the time-dependent seismic signal, $s(t)$, is modeled as the convolution of the primary reflectivity of the earth, $r(t)$, and an input signal (a wavelet), $w(t)$, as seen in equation 3.1. The model assumes normal incidence propagation in a horizontally layered earth where the layers are isotropic, elastic and homogeneous. Thus effects such as absorption, anisotropy, mode conversion and directivity are not explicitly included. A term representing additive noise associated with the seismic acquisition (from the recording equipment, environment, etc.), $n(t)$, is also often included in this model (Walden & White, 1998).

$$s(t) = r(t) * w(t) + n(t) \tag{3.1}$$

The reflectivity of the earth (reflectivity series) comprises a set of reflection coefficients, which give the proportions of the seismic wave amplitude that are reflected at each contrast in acoustic impedance. Acoustic impedance is defined for each earth layer as the product of velocity, V, and bulk density, ρ. The pressure reflection coefficient, R, is then expressed as in equation 3.2 where the velocities and densities of the upper and lower layers correspond to the ones in Figure 3.1 (Anstey, 1981). Furthermore, the wavelet in equation 3.1 is a time series representation of a seismic pulse, formally the waveform obtained from a single reflector of unit strength at a certain depth in the earth (White & Simm, 2003a).

$$R = \frac{\rho_2 V_2 - \rho_1 V_1}{\rho_2 V_2 + \rho_1 V_1} \tag{3.2}$$

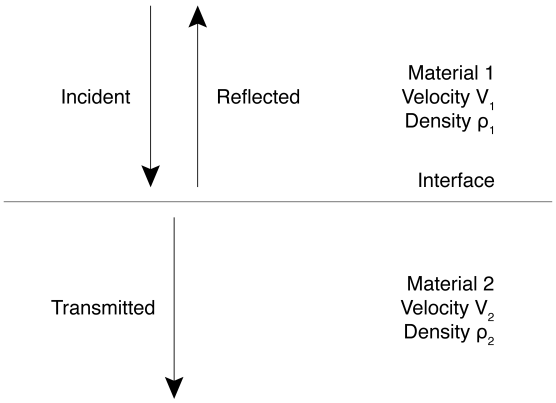

Figure 3.1: Two-layer earth model for a wave crossing an interface at normal incidence. After Anstey (1981).

A waveform can alternatively be uniquely defined in the frequency domain by its amplitude spectrum together with its phase spectrum. Any periodic waveform can be represented by a Fourier series, that is as a sum of sines and cosines where each component has its own frequency, amplitude and phase. A periodic function $f(t)$ with period T has a Fourier series of the form shown in equation 3.3, where the corresponding Fourier coefficients are given by equations 3.4, 3.5 and 3.6 (Kreyszig, 2006).

$$f(t) = a_0 + \sum_{n=1}^{\infty} \left(a_n \cos \frac{2\pi nt}{T} + b_n \sin \frac{2\pi nt}{T} \right) \tag{3.3}$$

$$a_0 = \frac{1}{T} \int_{-T/2}^{T/2} f(t)\, dt \tag{3.4}$$

$$a_n = \frac{2}{T} \int_{-T/2}^{T/2} f(t) \cos \frac{2\pi nt}{T}\, dt \quad (n = 1,\, 2,\, ...) \tag{3.5}$$

$$b_n = \frac{2}{T} \int_{-T/2}^{T/2} f(t) \sin \frac{2\pi nt}{T}\, dt \quad (n = 1,\, 2,\, ...) \tag{3.6}$$

Likewise, any transient waveform can be represented by a sum where the components occur with infinitesimally small frequency spacing, that is, in effect as a Fourier integral. The Fourier integral of a nonperiodic function $f(t)$ defined over the entire real line is given by equations 3.7, 3.8 and 3.9 (Kreyszig, 2006).

$$f(t) = \int_0^{\infty} [A(w) \cos wt + B(w) \sin wt]\, dw \tag{3.7}$$

$$A(w) = \frac{1}{\pi} \int_{-\infty}^{\infty} f(v) \cos wv \, dv \tag{3.8}$$

$$B(w) = \frac{1}{\pi} \int_{-\infty}^{\infty} f(v) \sin wv \, dv \tag{3.9}$$

Another useful application derived from the above formulas is that a function can be transformed to depend on a new variable, thus for instance a function defined in the time domain can be transformed into the frequency domain. Equation 3.10 gives the Fourier transform of $f(t)$, while equation 3.11 gives the inverse Fourier transform of $F(\omega)$ (Kreyszig, 2006). It now follows that the amplitude and phase spectra can be defined by equations 3.12 and 3.13, respectively (Gadallah & Fisher, 2005).

$$F(\omega) = \frac{1}{\sqrt{2\pi}} \int_{-\infty}^{\infty} f(t) \exp(-i\omega t) \, dt \tag{3.10}$$

$$f(t) = \frac{1}{\sqrt{2\pi}} \int_{-\infty}^{\infty} F(\omega) \exp(i\omega t) \, d\omega \tag{3.11}$$

$$A(\omega) = |F(\omega)| \tag{3.12}$$

$$\phi(\omega) = \arctan \frac{\operatorname{Im} F(\omega)}{\operatorname{Re} F(\omega)} \tag{3.13}$$

Figure 3.2 (a) shows an example of a wavelet comprising selected components with its amplitude spectrum presented in Figure 3.2 (b). Several traits can be observed from the amplitude spectrum of a wavelet, for instance a pulse dying quickly to zero will have less contribution from its end-frequencies and an amplitude spectrum with smooth and rounded corners. Wavelets with short and well resolved pulses typically display broader frequency bandwidths than do wavelets with longer pulses, while undulating amplitude spectra are typical for wavelets that have tendency toward repetition (Anstey, 1981).

The relative timing of the different components in a wavelet are controlled by the phase spectrum. Wavelets where all components have a phase of 0° are regularly referred to as zero phase wavelets, see Figure 3.2 (c). Such wavelets are symmetric about time zero as each component must have a peak centered at this time. Zero phase wavelets are usually the most desirable for seismic interpretation since the energy dominantly resides

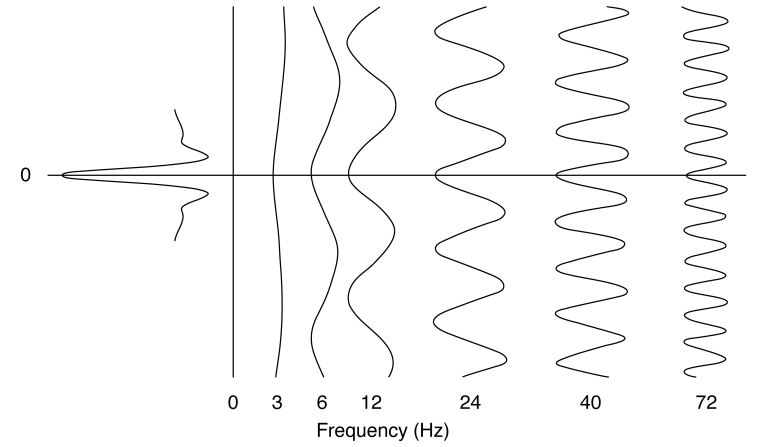

(a)

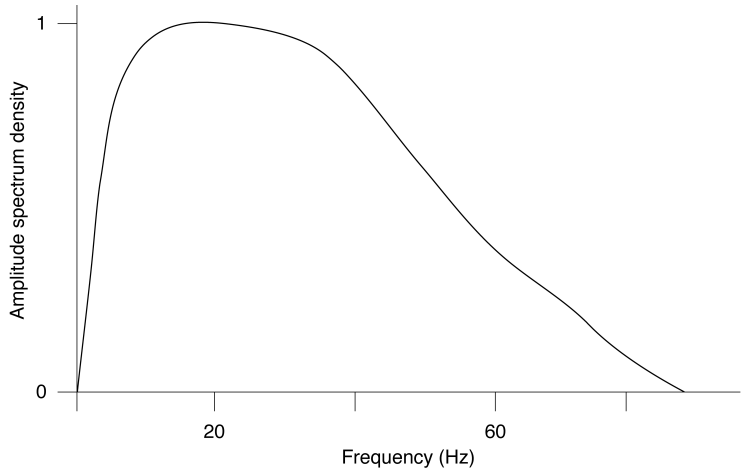

(b)

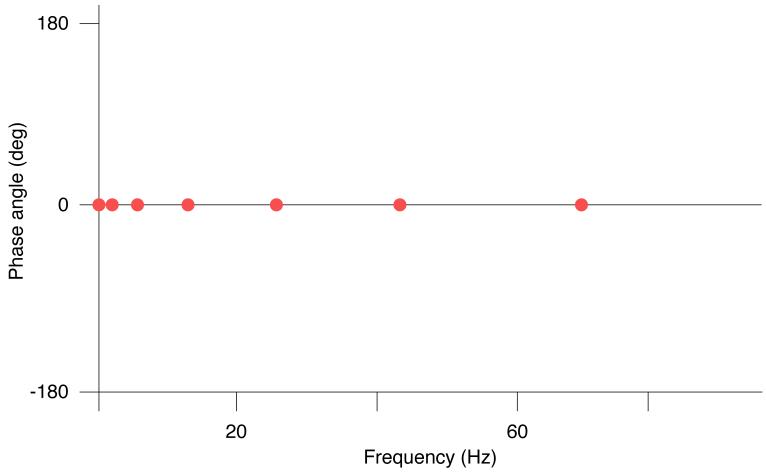

(c)

Figure 3.2: Different aspects of a zero phase wavelet. (a) Wavelet presented in the time domain together with the components of which it is made. Time zero is indicated by the horizontal line. (b) Amplitude spectrum. (c) Phase spectrum. After Simm & White (2002).

in the main lobe and reflections are more readily distinguished (Simm & White, 2002). Any other rectilinear phase spectrum that intercepts the phase axis at the origin or at an integral multiple of 360°, will retain the symmetric shape of the wavelet but impose a time delay or advance proportional to the slope of the phase spectrum. Therefore any symmetric wavelet that is not centered on time zero is, strictly speaking, not a zero phase wavelet but could instead be called a linear phase wavelet. Phase spectra that are neither zero phase nor rectilinear satisfying the above conditions, will however, result in an asymmetric wavelet with reduced amplitude that is time delayed or advanced and dispersed to occupy a greater time (Anstey, 1981).

3.2 Seismic well ties

The convolutional model (section 3.1) forms the foundation for the procedure of seismic well ties. Reflection seismic data are typically acquired over a broad area aiming at understanding a region of the subsurface. Well log measurements, on the other hand, are made only in the vicinity of a borehole with the aim of understanding the local area. Compared to seismic recordings, well log data have higher depth resolution and contain more detail on the situation in the earth. Both types of measurements are often acquired in an area of interest, and being able to establish which seismic reflectors that correspond to which well log responses is critical for our understanding and application of the data. This connection between seismic and well log measurements is accomplished through seismic well ties.

The basic principle of a seismic well tie is to create a synthetic seismic trace (synthetic seismogram) using well logs and compare this with the recorded seismic traces surrounding the location of the well. A common approach for establishing a representative reflectivity series is to calculate reflection coefficients from the sonic (formation velocity) and density logs. However, the traveltimes obtained through integration of sonic logs commonly deviate from reflection seismic traveltimes due to differences in the nature of the experiments. Thus it is necessary to calibrate the sonic log using a known time-depth relationship for integrated sonic log traveltimes to agree with seismic traveltimes. A time-depth relationship can be obtained from seismic recordings such as checkshot surveys or zero offset Vertical Seismic Profiles (VSPs), measured in the vicinity of the well (White & Simm, 2003a).

The wavelet with which to perform the well tie can be chosen or determined in many different ways. For example, a wavelet could be designed by applying earth filter effects

to the far-field source signature response modeled or measured from the seismic acquisition system. Another approach is to construct a zero phase wavelet with a similar energy spectrum to that of the seismic data to be used in the well tie, and manually time shift and phase rotate it until the optimal match between the two is reached (White & Simm, 2003a). For the case when reasonable quality well log data are available however, a pragmatic and quantitative approach to extracting the wavelet is through a least squares matching technique (section 3.3) in which the wavelet is estimated directly from the seismic (White, 1980). Idealized wavelets such as Ricker wavelets or Butterworth wavelets can also be used as the input signal, but would likely give less accurate well ties with typical seismic data. The wavelet is then convolved with the reflectivity series to generate the synthetic seismogram, and the seismogram is compared with the reflection seismic as shown in Figure 3.3.

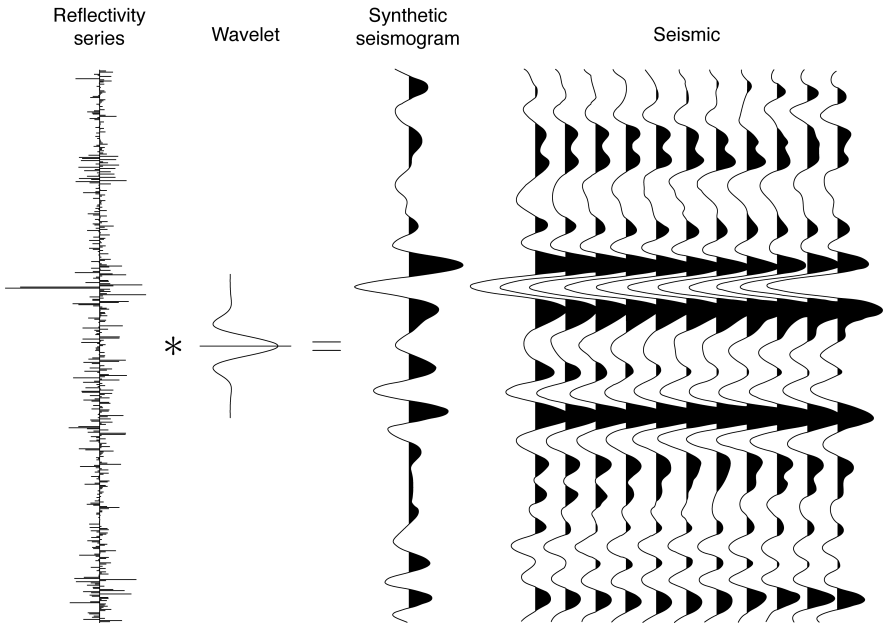

Figure 3.3: Principle of the seismic well tie. The reflectivity series is convolved with a wavelet to produce a synthetic seismogram. The seismogram is then compared to the reflection seismic. Time zero relative to the wavelet is indicated by the solid line.

The well tie is usually performed over a limited time window rather than the entire depth extent of the well logs, as the quality and characteristics of the data typically change with time. Moreover, many well tie software packages offer the option to stretch or squeeze parts of (or whole of) the synthetic seismogram to improve the correlation between the synthetic and the reflection seismic. Although this might visually give more agreeable well ties, there is rarely any physical foundation supporting such an action.

Stretching and squeezing should be avoided as it in effect modifies the data and reduces the reliability of the well tie (White et al., 1998). The general steps usually included in a well tie procedure may thus be summarized as follows:

1. Quality control, and if necessary edit, input well logs. Quality control seismic data.
2. Specify an input time-depth relationship approximating the correct well log placement in time.
3. Calibrate the sonic log for the log times to agree with seismic times.
4. Construct a reflectivity series from calibrated sonic and density logs.
5. Establish parameters with which to estimate the wavelet that optimally describes the input signal.
6. Generate the synthetic seismogram by convolving the obtained wavelet with the reflectivity.
7. Compare the synthetic seismogram with the reflection seismic.

3.3 Ordinary coherence wavelet estimation

An effective and robust approach to estimating a wavelet for seismic well ties (section 3.2) is through a coherency matching technique described by White (1980). In this technique the aim is to obtain, for a given set of parameters, the wavelet that when convolved with the reflectivity series provides the best match with a given seismic trace in a least squares sense. Several time gates and several seismic traces around the well are scanned for the best match location in a specified time window. The solution obtained is the frequency response of the wavelet, $W(f)$, as the ratio of the cross-spectrum of the synthetic and the seismic trace, $\Phi_{xy}(f)$, over the power spectrum of the synthetic, $\Phi_{xx}(f)$, as seen in equation 3.14 (White, 1980). The wavelet can then be found by Fourier synthesis and statistical measures can be applied to ascertain the reliability of the tie.

$$W(f) = \frac{\Phi_{xy}(f)}{\Phi_{xx}(f)} \tag{3.14}$$

The seismic trace at the given well location is not necessarily the optimal trace with which to perform the well tie. For instance, for time migrated data in the presence of significant dip, the best match location will typically have moved up-dip from the well (White & Simm, 2003a). The power and cross-spectra used in the matching should also be smoothed by a spectral window (Walden & White, 1984). The quality of the match between the synthetic seismogram and the seismic trace can be quantified by

the ordinary coherence, $\gamma^2(f)$, computed as shown in equation 3.15 (White, 1980). This function is a measure of goodness-of-fit as it estimates the extent to which the seismic trace may be predicted by linearly filtering the reflectivity series. An alternative measure of goodness-of-fit is the square of the correlation coefficient, which for an error-free synthetic is equivalent to the predictability, P (White & Simm, 2003a). Values for P range between 0-1 where a value of 1 signifies an ideal match in that the seismic trace is completely reconstructed by a filtered version of the reflectivity series.

$$\gamma^2(f) = \frac{|\Phi_{xy}(f)|^2}{\Phi_{xx}(f)\Phi_{yy}(f)} \tag{3.15}$$

The accuracy of the synthetic seismogram is given by its normalized mean square error, *NMSE*, as the ratio between the energy in the errors in the synthetic and the energy in the synthetic itself. Energy is here defined as the sum of the squared amplitudes of a time series. As this measure assumes knowledge about the ideal synthetic seismogram (which one rarely has), *NMSE* should in practice be approximated by its expected value as given in equation 3.16 (White & Simm, 2003a), where b is the bandwidth of the smoothing window applied to the seismic and the synthetic, and T is the length of the time window. A good well tie will then have a value of $P > 0.7$ and an $NMSE < 0.1$ (Simm & Bacon, 2014). This approximation is also valid for the *NMSE* of the wavelet assuming a rather flat reflectivity spectrum.

$$E\{NMSE\} = \frac{1}{bT}\frac{1-P}{P} \tag{3.16}$$

The smoothing window bandwidth can be defined as in equation 3.17 (Percival & Walden, 1993), where Δt is the sampling interval of the data, w_τ is the lag window (the inverse Fourier transform of the smoothing window), and N is the sample size. The equation requires that the smoothing window is an even $2f_{(N)}$ periodic function with $w_0 = 1$. The mean standard error in phase of the wavelet, $\phi(f)$, is related to the *NMSE* as shown in equation 3.18 (White & Simm, 2003a). As a general guideline a tolerable phase error might be $< 30°$ for wavelets used in seismic well ties, $< 20°$ for AVO modeling and $< 10°$ for seismic inversion (White, 1997).

$$b = \frac{1}{\Delta t \sum_{\tau=-(N-1)}^{N-1} w_\tau^2} \tag{3.17}$$

$$S.E.\{\phi(f)\} \simeq \sqrt{\frac{NMSE}{2}} \quad \text{(rad)} \tag{3.18}$$

An advantage of using coherency matching for wavelet estimation is that it makes no assumptions about wavelet timing, amplitude or phase, while noise is assumed to be random and stationary. However, the wavelet length with which to perform the technique needs careful consideration. A sufficiently short wavelet would more likely be biased (distorted), while longer wavelets tend to include more noise into the estimation thus matching with noise as well as the seismic signal. As biasing errors get more severe with decreasing wavelet length than errors due to inclusion of noise with increasing length, one should err towards longer rather than shorter wavelets (White & Simm, 2003a).

The timing and phase angle of a wavelet extracted from seismic is sensitive to the data bandwidth. White & Simm (2003b) showed that the likelihood of estimating a unique wavelet for a well tie decreased with decreasing bandwidth. Statistical bandwidth of data can be estimated by equation 3.19 (Wang, 2003), where $C_{xx}(\tau)$ is the sample autocovariance of the time series, T is the time window, and w_τ is a lag window. An approximately unbiased estimate is then obtained by equation 3.20, where ν is the degrees of freedom of w_τ. The ordinary coherence wavelet estimation technique can further be expanded by treating the differing contributions to the seismic signal (such as primaries, surface multiples, internal multiples, etc.) as separate components. The technique is then partial/multiple coherence wavelet estimation (White, 1980), and might be relevant for situations where seismic well ties are performed at an early stage of seismic processing and internal multiples have yet to be removed.

$$\hat{B} = \frac{C_{xx}(0)^2}{2\sum_{\tau=-(T-1)}^{T-1}\left(1-\frac{|\tau|}{T}\right)w_\tau^2 C_{xx}(\tau)^2} \tag{3.19}$$

$$B = \left(1+\frac{2}{\nu}\right)\hat{B} - \frac{1}{T} \tag{3.20}$$

3.4 Seismic attenuation

For anelastic and inhomogeneous media in the earth, a significant factor that will affect both the amplitude and phase of a seismic signal is seismic attenuation, which includes dissipation of seismic energy through absorption and scattering. The energy of a seismic wave is absorbed by the medium through which it propagates and ultimately the energy is converted into heat. Scattering can occur due to fine layering in the earth or from small heterogeneities, and produces effects on seismic data which might be difficult to separate from the effects of absorption. A plane wave propagating in the positive x-direction at

traveltime t in an elastic and homogeneous medium can be described by equation 3.21, where f is the frequency and k is the wavenumber of the wave. To introduce the effect of attenuation on a wave, k should be replaced by a complex wavenumber, κ, which includes in its imaginary part an attenuation coefficient, α, as seen in equation 3.22 (Wang, 2008). The wave can then be described by equation 3.23.

$$U(x,t) = U_0 \exp[i(2\pi f t - kx)] \tag{3.21}$$

$$k = \kappa - i\alpha \tag{3.22}$$

$$U(x,t) = U_0 \exp[i(2\pi f t - \kappa x)] \tag{3.23}$$

The attenuation coefficient quantifies how quickly energy is absorbed by a medium. The seismic quality factor, Q, is a material property that gives the ratio of stored energy, E, to dissipated energy, ΔE, per cycle of harmonic loading. Q can thus be defined as shown in equation 3.24 (Sheriff & Geldart, 1995). For a plane wave in a horizontally layered medium Q is related to the attenuation coefficient by equation 3.25 (Wang, 2008) where V is the constant speed of the wave propagation. Therefore the attenuation coefficient is roughly linearly dependent on frequency, and Q^{-1} signifies how much attenuation there is. The lower the value of Q, the more attenuative the medium. Q is a dimensionless quantity and typical values for less attenuative media are 500-1000, while typical values for highly attenuative media are 10-100 (Gusmeroli et al., 2010). Q values applied in Q-compensation during processing of seismic data usually include effects of both absorption and scattering.

$$Q = \frac{2\pi E}{\Delta E} \tag{3.24}$$

$$\alpha \approx \frac{\pi f}{VQ} \tag{3.25}$$

Attenuation affects seismic by exponentially reducing the amplitudes of higher frequency components compared to the amplitudes of lower frequency ones of a wave propagating through the earth. Thus higher frequency components will be attenuated at a higher rate than lower frequency ones. Amplitude-only Q-compensation applied to seismic data during processing aims at recovering the amplitude information lost due to attenuation. Furthermore, absorption must be accompanied by velocity dispersion to satisfy the criteria of linearity and causality in wave propagation (Futterman, 1962). Thus lower frequency components will travel slower than higher frequency components resulting in wavelet delay and distortion. Phase-only Q-compensation aims at correcting for the

effects of velocity dispersion. Phase-only and amplitude-only Q-compensation can be performed simultaneously or separately.

Following the above discussion velocity depends on frequency, $V(f)$, as velocity dispersion must be present in an attenuative medium. Q is also dependent on frequency, but by choosing an appropriate attenuation coefficient and associated phase velocity (an attenuation-dispersion pair), Q can be assumed effectively constant over the seismic frequency range (Aki & Richards, 2002). The attenuation and phase operators used in this study are given by equations 3.26, 3.27 and 3.28 (Ferber, 2005), where sgn is set as either sgn $= -1$ or sgn $= 1$ depending on whether Q is to be forward or inverse modeled, respectively. A reference frequency is also specified as f_{ref} (section 3.5), and t^* is the ratio of traveltime and Q. A model where Q is dependent on traveltime might be appropriate to include when using these equations, depending on the purpose of the modeling. The summary about seismic attenuation in this section was largely obtained from a previous student project by Czajkowski (2014).

$$A_{t^*}(f) = \exp(\operatorname{sgn} \pi f t^*) \tag{3.26}$$

$$\phi_{t^*}(f) = \operatorname{sgn} 2f \ln\left(\frac{f_{ref}}{f}\right) t^* \tag{3.27}$$

$$t^* = \frac{t}{Q(t)} \tag{3.28}$$

3.5 Phase-only Q-compensation

The result of velocity dispersion is to time shift and phase distort the wavelet. Phase-only Q-compensation is performed with the purpose of producing zero phase seismic data correcting for the frequency dependence of velocity. This helps accurate interpretability and timing of the seismic, giving a better correlation with well log data. The correction is applied following the designature and debubble steps that zero phase the source wavelet during seismic processing. The choice of reference frequency used in phase-only Q-compensation is important to the outcome. The velocity at which this frequency component travels will be the velocity to which the velocities of all other frequency components will be adjusted.

For a relationship between phase velocity and frequency as shown in Figure 3.4, letting the reference frequency, f_{ref}, travel at velocity V, all higher frequency components will be slowed down and all lower frequencies will be sped up to this velocity. Choosing a higher reference frequency signifies that seismic will be time shifted to earlier arrival

times, while choosing a lower reference frequency will time shift seismic to later arrival times. The opposite is true for forward Q modeling. Phase-only Q-compensation thus lets all frequency components travel at the same velocity V, allowing for symmetric and zero phased seismic wavelets. Note that Statoil's current best practice is to set the reference frequency to the dominant frequency at top reservoir on surface seismic. In this way the stratigraphy above and below the reservoir might be time shifted, but top reservoir would still occur at the correct traveltimes.

Q can be estimated from both VSP data and surface seismic data. It is rather difficult to estimate Q, and some residual phase error will likely still be present in the wavelet after correction. A precise estimation of Q is however not required to remove most of the effects of velocity dispersion in the subsurface, and as long as Q is overestimated the residual error will not be larger than the original dispersion in the data (Duren & Trantham, 1997). The effects of overcorrecting or undercorrecting seismic data are shown in Figure 3.5. In either case the resulting wavelet is asymmetric with differing sidelobes.

Phase-only Q-compensation is usually applied to pre-stack data as attenuation is offset-dependent and the different corrections may be needed for each trace. A stacked trace gives a mean of all the traces involved and stacking phase distorted and time shifted wavelets would give incorrect results. Also, as water is a nearly non-dispersive and non-attenuative medium, phase-only Q-compensation should not be applied to the water layer in offshore seismic data. The summary about phase-only Q-compensation in this section was in large part obtained from a previous student project by Czajkowski (2014).

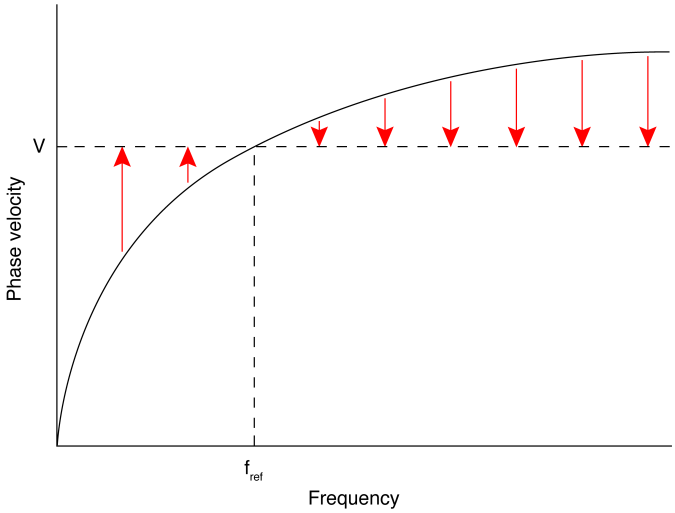

Figure 3.4: A typical phase velocity dispersion curve. The arrows show the effect of a phase-only Q-compensation on phase velocity given the reference frequency. This assumes the use of the correct Q value in the Q-compensation. After Czajkowski (2014).

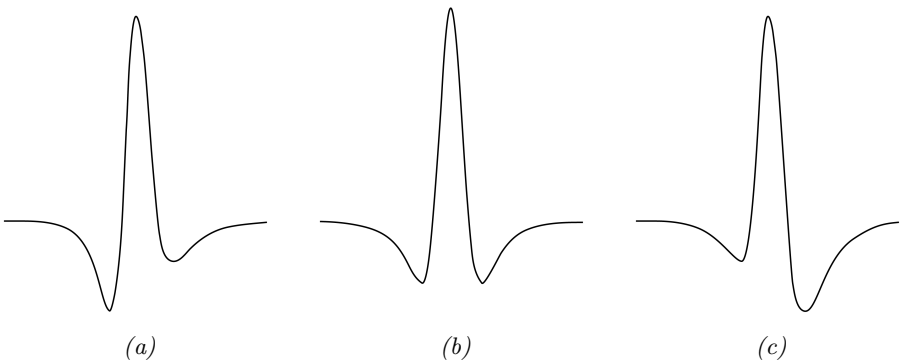

Figure 3.5: Shape of originally seismic zero phase 3-lobe wavelets expected for (a) an undercorrection where Q was too high, (b) an optimal case where Q was just right, and (c) an overcorrection where Q was too low. After Czajkowski (2014).

4

Datasets and Software

A receiver-deghosted Geostreamer® 3D seismic survey (MC3D-HVG2013) was used for this study, acquired and processed by Petroleum Geo-Services (PGS) in 2013. The key acquisition parameters are given in Table 4.1. A particularly relevant step during processing was the phase-only Q-compensation applied pre-stack. The Q-compensation was performed immediately prior to migration velocity analysis with a constant Q value of 135 and a reference frequency of 35 Hz starting from the seabed. Other processing steps important for the phase of the data included receiver deghosting, and a designature to zero phase, such that a peak on the seismic would represent an increase in acoustic impedance. Significant processing steps for the bandwidth of the data were the receiver deghosting, a receiver-based bandwidth optimization, a post-stack source bandwidth optimization, and an amplitude only Q-compensation performed with $Q = 120$ starting from the seabed. A full-stack seismic volume was used in this experiment.

Well logs from exploration well 6506/12-3 from the Åsgard field were also used. The well was drilled to a total depth of 4338 m (ending in the Tilje Formation) including a water depth of 301 m (Jensen et al., 1985). Due to washout zones in the shales at Jurassic reservoir levels, poor borehole wall coupling significantly affected the well log measurements. The well logs used in this study have however both been edited and quality controlled (Figure 4.1). Matlab R2012b was used for forward and inverse Q modeling, for generating plots of results and for general calculations. Seismic well ties and wavelet extractions were performed using the software Petrel 2014.5. Seismic Unix was used to convert data from one format to another, and for amplitude gain corrections.

Table 4.1: Key acquisition parameters for MC3D-HVG2013 (Urbanek, 2014)

Parameter	**Value**
Source depth	8 m
Source volume	2x4130 in^3
Source pressure	2000 psi
Number of streamers	14
Group interval	12.5 m
Cable length	7050 m
Cable depth	20 m
Recording length	7680 ms
Sampling interval	2 ms

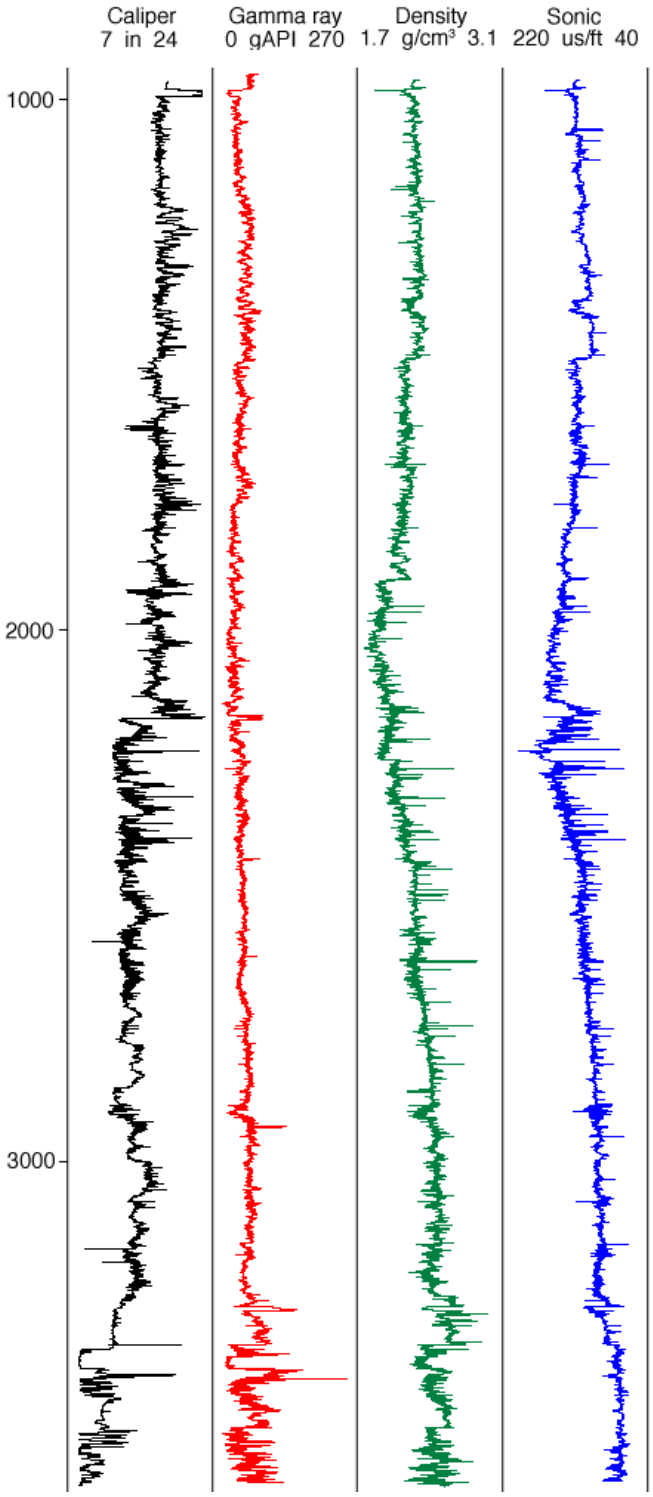

Figure 4.1: Well logs from well 6506/12-3.

5

Forward Q modeling phase effects on a well tie using synthetic data

5.1 Experimental methods

This experiment achieved to assess the detectability of Q effects on a seismic well tie using synthetic data. If the effects were undetectable on synthetic data, it would be unnecessary to perform a similar experiment on real data. Another motivation for performing this experiment was to check to which degree the software was suitable for wavelet extractions, and also to establish what parameters to use for wavelet extractions with a known result. The time-depth relationship applied in this experiment was one prepared by Statoil according to their best practice (TIME-CKS). Furthermore, the sampling interval of all data generated in this test was set to 1 ms to simulate best case scenarios. A reflectivity series was first constructed using the sonic and density logs from well 6506/12-3 in Petrel. The result was then convolved with a 128 ms long zero phase Butterworth wavelet to produce a synthetic seismic trace. The Butterworth wavelet was made deliberately broad to simulate an ideal seismic trace with a large bandwidth. The low slope was thus set to 18 dB/Octave, the high slope to 72 dB/Octave, and the frequency content was set to range between 5-150 Hz.

The synthetic seismic trace was loaded into Matlab where both phase and amplitude forward Q modeling was applied according to equations 3.26, 3.27 and 3.28 (Ferber, 2005). Starting from time zero the water layer was modeled with $Q = 10\ 000$, while the sediments were modeled for cases with $Q = 50$ and a reference frequency of 35 Hz, and $Q = 135$ and reference frequencies of 1 Hz, 35 Hz, 50 Hz and 100 Hz. The high

Q value for the water layer was chosen so as to model a non-attenuative layer. For the sediments a Q of 50 was used to ensure a case where the effects of attenuation and dispersion would be evident, while a Q of 135 as it was the value with which the seismic survey MC3D-HVG2013 had been processed (Urbanek, 2014). The reference frequencies were chosen with the intent of representing the range of frequencies in a typical seismic experiment.

The algorithm used first calculated t* and constructed a filter bank gather following Ferber (2005). Each filter was then applied in turn to the synthetic seismic trace in the frequency domain, creating a gather of filtered traces. The Q modeled output trace was calculated by interpolating between the t* values for the required time sample from each trace in the gather. This code was written by the thesis supervisor specifically for this student project. From each output trace a 3x3 synthetic seismic cube was constructed such that all the traces in a cube were identical.

To mitigate the effects of amplitude forward Q modeling on the peak amplitude decay of the traces, frequency-independent amplitude gain correction was applied to each cube through Seismic Unix. The thought was to improve the stationarity of the traces for the subsequent seismic well ties, and to better be able to assess the phase Q effects. The data were thus multiplied by $\exp(\pi f_{gain} t/Q)$ derived from equation 3.26 (Ferber, 2005), as the amplitude forward Q modeling already applied also was based on this equation. The corrections were done with f_{gain} values of 15 Hz and 30 Hz for the cubes modeled with $Q = 50$ and $Q = 135$, respectively. The given frequencies were chosen after performing well ties testing several values. A synthetic cube without any forward Q modeling was additionally created from the initial synthetic seismic trace. The cubes were then imported into Petrel where seismic well ties were performed for a window between 2800-3582 ms.

Forward Q modeling was also applied to the Butterworth filter itself with $Q = 50$ and a reference frequency of 35 Hz, and with $Q = 135$ and reference frequencies of 1 Hz, 35 Hz, 50 Hz and 100 Hz. The filter was shifted and zero padded prior to the modeling such that the peak of the wavelet was positioned approximately in the center of the well tie window at 3200 ms. The purpose was to generate the ideal seismic signal obtained from a Q modeled isolated reflector at this depth. These waveforms show what the wavelets extracted from the well ties with the synthetic cubes should ideally be.

A seismic well tie was first performed for the cube that had not undergone any Q modeling. A synthetic seismogram was constructed using the sonic and density logs from

well 6506/12-3 and a 256 ms wavelet, extracted from the seismic cube using ordinary coherence matching as outlined by White (1980). As the cube did not include any effects of Q, it was expected to extract the same Butterworth filter which had initially gone into the synthetic trace. This test was performed to assess how accurately the well tie software could extract the input wavelet, to learn how to parametrize the extraction, and to asses whether it is at all possible to extract similar wavelets from such a well tie.

Seismic well ties were subsequently performed for each of the forward Q modeled seismic cubes, using the same well logs as earlier from well 6506/12-3 as input to the synthetic seismograms. The ideal wavelets obtained from Q modeling the Butterworth filter helped establish a consistent set of parameters with which to carry out the ordinary coherence wavelet estimations. As all traces within a given cube were the same extractions could be performed from either trace. The reflectivity series was then scanned with a time gate of 40 ms so that an extracted wavelet would not be allowed to deviate more than 20 ms from the seismic. The parameters used are summarized in Appendix A.1. Thus the resulting wavelets would only differ due to dissimilarities between the synthetic seismic cubes from which they were extracted.

512 ms long wavelets were extracted for each seismic well tie and loaded into Matlab for analysis. The original Butterworth wavelet was compared with the wavelet extracted from the cube without any Q modeling. The wavelet estimated from the seismic modeled with $Q = 50$ and reference frequency 35 Hz was compared with the corresponding ideal wavelet obtained by Q modeling the Butterworth filter. Finally all wavelets extracted from Q modeled seismic were compared against each other. The amplitude and phase spectra were also compared for each of the above cases. Frequency bandwidths for the well tie time window were estimated over each wavelet extraction trace using a propriety software provided by Statoil based on equations 3.19 and 3.20 (Wang, 2003). For each input TWT the software calculated the corresponding frequency bandwidth over an 782 ms time window centered on the given time value. The results were plotted.

5.2 Results

These results test the detectability of Q effects on wavelets extracted in seismic well ties using synthetic data. In this experiment a synthetic seismic trace was generated by convolving a reflectivity series with a broad bandwidth zero phase Butterworth wavelet. Phase and amplitude forward Q modeling was then performed with $Q = 50$ and a reference frequency of 35 Hz, and with $Q = 135$ and reference frequencies of 1 Hz,

35 Hz, 50 Hz and 100 Hz. From each Q modeled trace a synthetic seismic cube was constructed and amplitude gain corrections were applied. Additionally, the Butterworth filter itself was forward Q modeled for each case to get the ideal seismic signal expected from an isolated reflector.

The final traces making up each of the seismic cubes are shown in Figure 5.1 for comparison. A clear distinction can be made for the case of no Q modeling applied and for Q modeling with $Q = 50$, but the differences between the traces modeled with $Q = 135$ are small. Seismic well ties were performed for every case using the synthetic cubes as input reflection seismic. The synthetic seismograms were created from the same reflectivity series and wavelets estimated from the seismic using ordinary coherence matching (White, 1980). The resulting wavelets from each seismic well tie, as well as their amplitude and phase spectra, were plotted for comparison.

The plot in Figure 5.2 shows that the initial Butterworth wavelet used to create the synthetic seismic trace is very similar to the extracted wavelet for the case where no Q modeling was applied. Figure 5.3 shows that the amplitudes of the input Butterworth wavelet are somewhat larger than for the extracted wavelet, with marginally sharper corners on the amplitude spectrum. The extracted wavelet has less contribution from its end-frequency components, thus dying out more quickly to zero. In both cases a broad range of frequencies is represented where amplitudes start to die out at around 200 Hz.

The phase spectra of these wavelets are shown in Figure 5.4. The phase of the input Butterworth wavelet is close to zero for frequencies up to 150 Hz, after which it oscillates about zero by a gradually increasing moment. For the extracted wavelet, the phase is nearly zero in the interval between 50-150 Hz. It differs from zero by a maximum of approximately 8° for lower frequencies, while it increasingly deviates from zero for larger ones. Generally the software successfully retrieved a wavelet comparable to the input Butterworth. The similarity between the two is high both in the time domain and in the frequency domain. Note however that as the wavelet amplitudes gradually decrease to zero, the reliabilities of the phase spectra also decrease as the phase spectra become unstable and the software experiences difficulties in interpreting them.

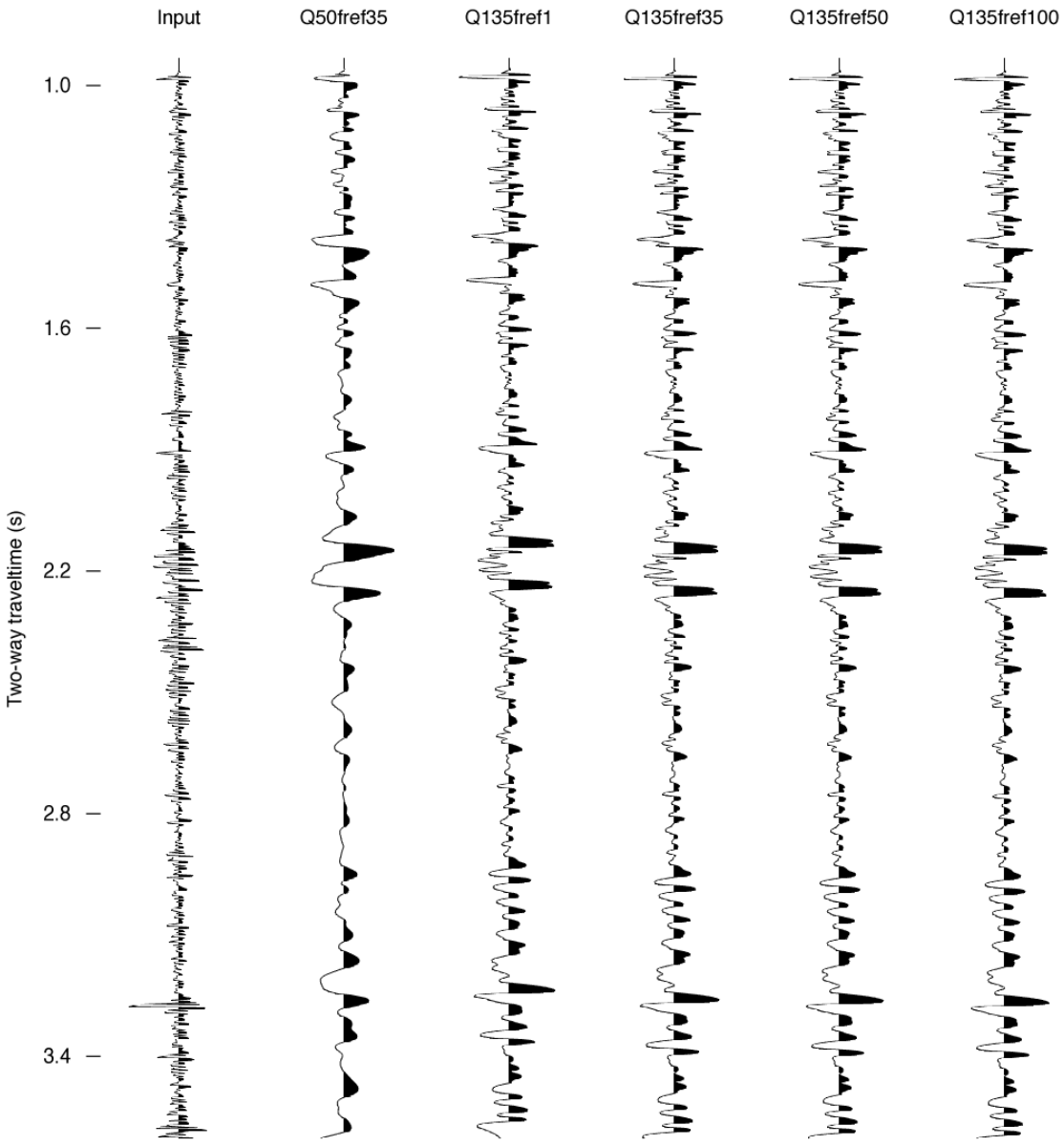

Figure 5.1: Synthetic traces that make up synthetic cubes for the case of no forward Q modeling applied, forward Q modeled with Q = 50 and reference frequency 35 Hz, and Q = 135 with reference frequencies 1 Hz, 35 Hz, 50 Hz and 100 Hz.

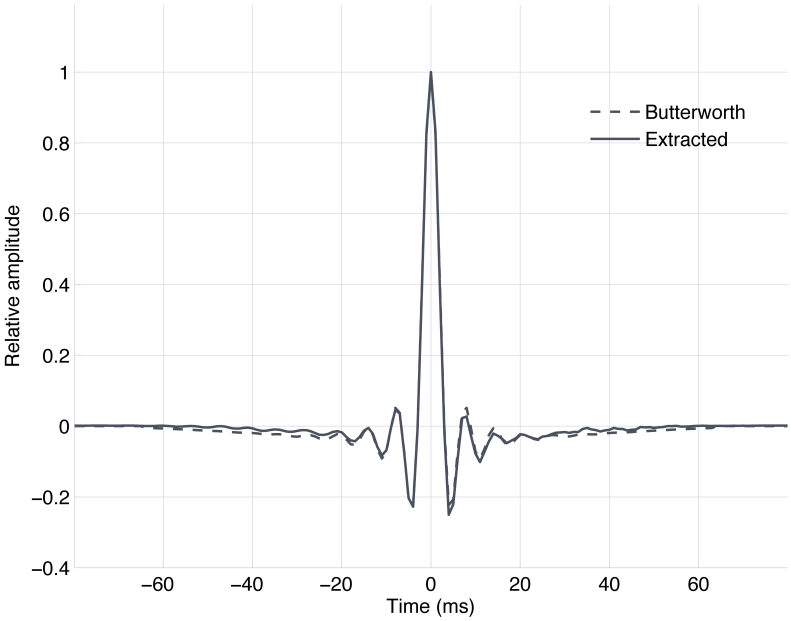

Figure 5.2: Input Butterworth wavelet and wavelet extracted from synthetic seismic without any Q modeling. Peak amplitudes have been scaled to unity.

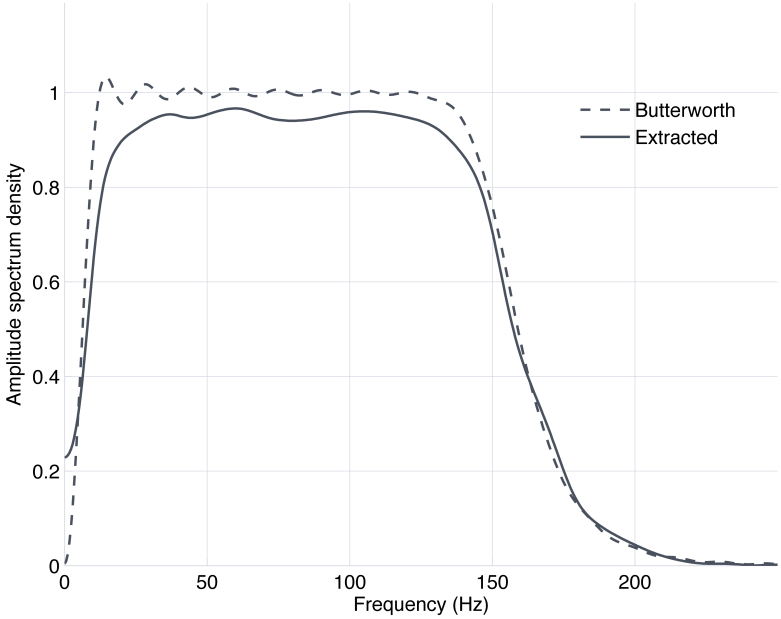

Figure 5.3: Amplitude spectra of the input Butterworth wavelet and the wavelet extracted from the synthetic seismic without any Q modeling.

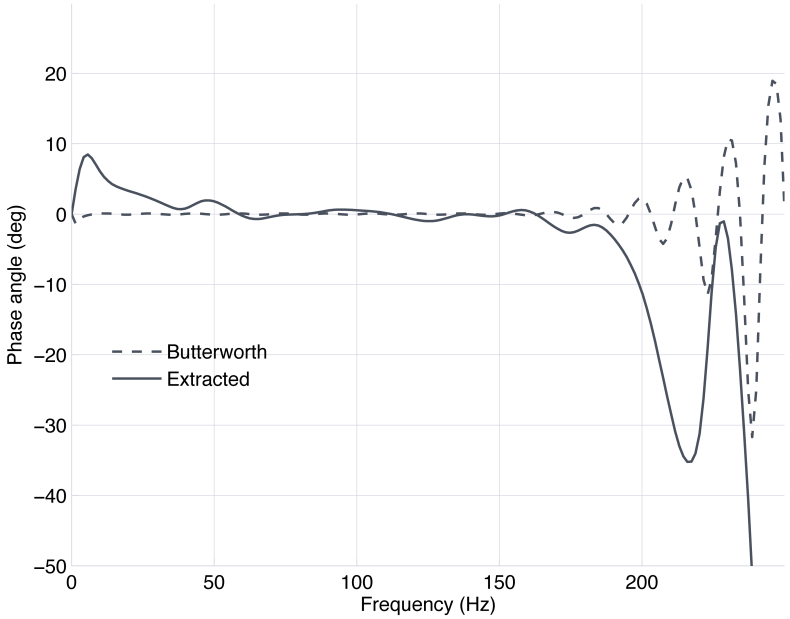

Figure 5.4: Phase spectra of the input Butterworth wavelet and the wavelet extracted from the synthetic seismic without any Q modeling.

Figure 5.5 compares the ideal wavelet obtained by forward Q modeling the Butterworth filter with the corresponding wavelet extracted from forward Q modeled synthetic seismic. In this example, both the Butterworth filter and the synthetic seismic were modeled with $Q = 50$ and a reference frequency of 35 Hz. The wavelets are highly asymmetric with a common central peak delayed relative to time zero. This delay was anticipated as the synthetic seismic now included attenuation effects. The extracted wavelet has more sidelobes than the ideal wavelet, and seems to decay more slowly towards zero. Nevertheless, this wavelet seems to be an adequate approximation to the ideal one for the purpose of these well ties.

The amplitude spectrum of the extracted wavelet in Figure 5.6 is considerably larger than for the ideal wavelet. This shows the effect of the amplitude gain correction that was applied to all synthetic seismic cubes, but which was not applied to the ideal wavelets. The shapes of the amplitude spectra are comparable, with peaks at approximately 7-8 Hz and amplitudes dying out close to zero at around 40 Hz. Furthermore, Figure 5.7 shows how both phase spectra gently curve downwards from 0°, before turning upwards to intercept the abscissa at approximately 35 Hz. This result was expected as the reference frequency was 35 Hz, thus letting this frequency component have a phase of 0°. The curved spectra are also evident from the asymmetry of the wavelet in Figure 5.5, as only zero phase or rectilinear spectra should give symmetric wavelets.

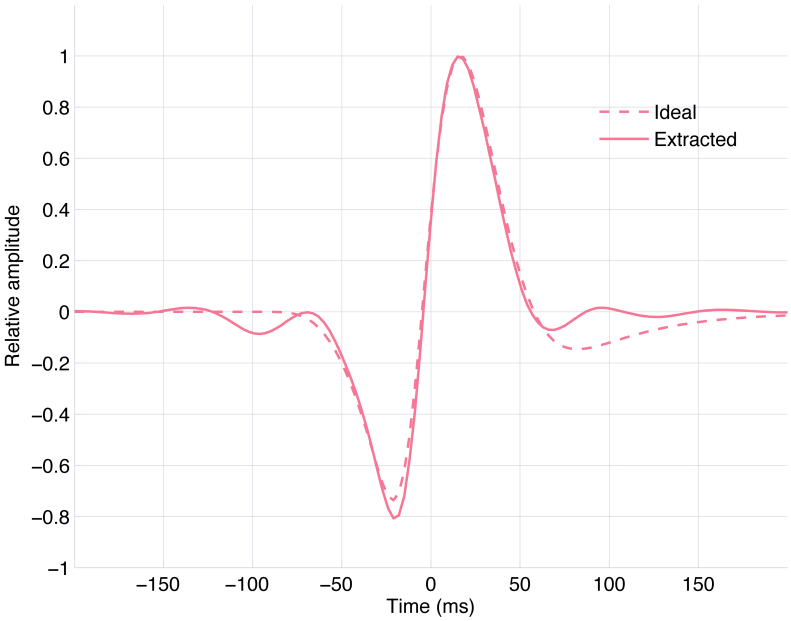

Figure 5.5: Ideal wavelet obtained by forward Q modeling the Butterworth filter and wavelet extracted from forward Q modeled synthetic seismic, for Q = 50 and a reference frequency of 35 Hz. Peak amplitudes have been scaled to unity.

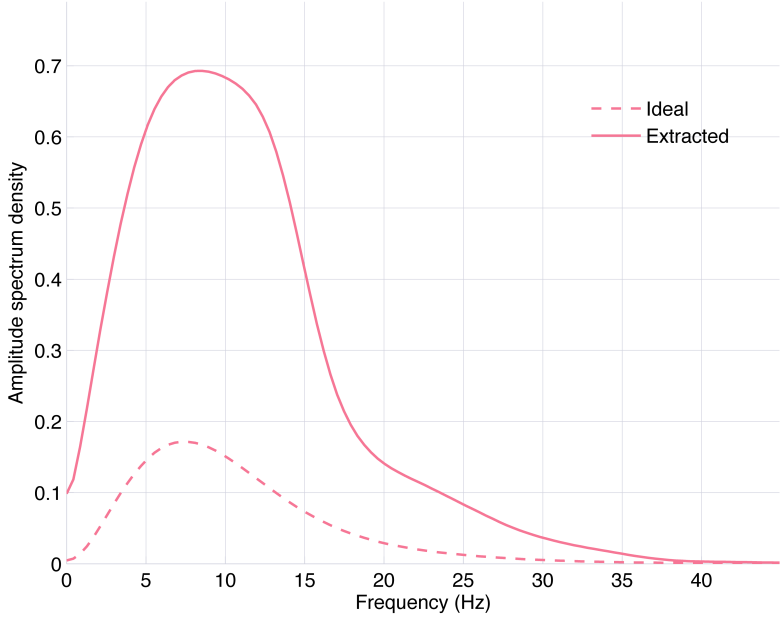

Figure 5.6: Amplitude spectra of the ideal wavelet obtained by forward Q modeling the Butterworth filter and of the wavelet extracted from forward Q modeled synthetic seismic, for Q = 50 and a reference frequency of 35 Hz.

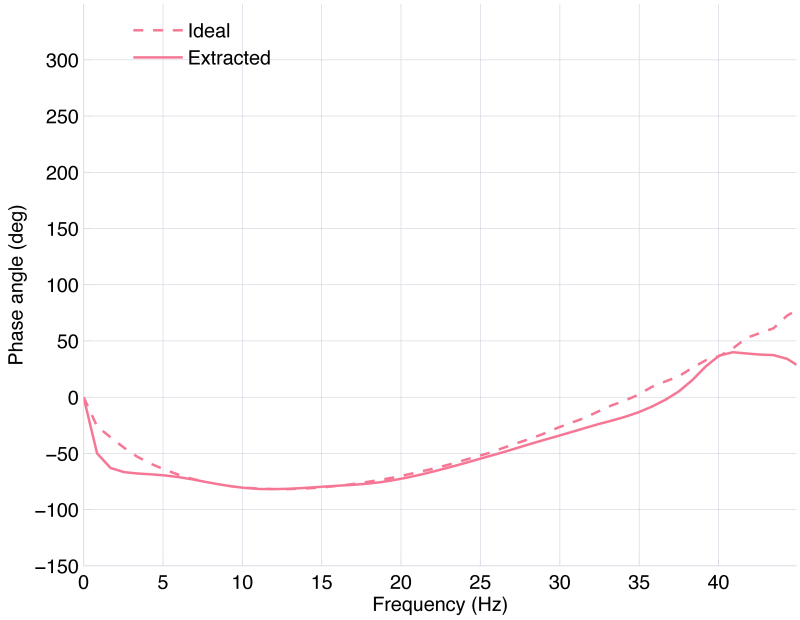

Figure 5.7: Phase spectra of the ideal wavelet obtained by forward Q modeling the Butterworth filter and wavelet extracted from forward Q modeled synthetic seismic, for $Q = 50$ and a reference frequency of 35 Hz.

All extracted wavelets from forward Q modeled synthetic seismic are shown in Figure 5.8, that is for $Q = 50$ and a reference frequency of 35 Hz, and for $Q = 135$ and reference frequencies 1 Hz, 35 Hz, 50 Hz and 100 Hz. The wavelet for $Q = 135$ and a reference frequency of 1 Hz is leading relative to time zero, while the peak of the wavelet modeled with the same value for Q and a reference frequency of 35 Hz seems to be centered on time zero. The remaining wavelets for this value of Q are increasingly delayed with higher reference frequencies. The wavelet for $Q = 50$ and reference frequency 35 Hz is the most delayed, and is also somewhat broader compared to the other wavelets. All wavelets are asymmetric, with the wavelet for $Q = 50$ displaying the most asymmetry.

Thus this comparison shows that forward Q modeling with sufficiently high reference frequencies will impose a delay on a wavelet, as the majority of the frequency components are lower than the reference frequency and are forced to travel with slower velocities than that of the reference frequency. Likewise, forward Q modeling with a very low reference frequency will give leading wavelets as the majority of the components in the wavelet travel with higher velocities than the that of the reference frequency. The plot also shows the effect of forward Q modeling with different values for Q, that is a low value will cause the wavelet to be more attenuated.

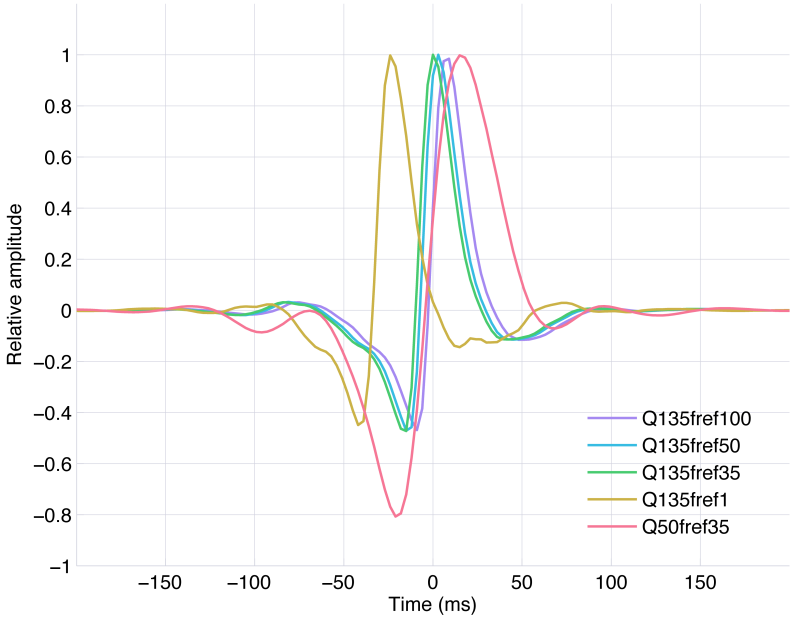

Figure 5.8: Wavelets extracted from forward Q modeled synthetic seismic with $Q = 50$ and a reference frequency of 35 Hz, and with $Q = 135$ and reference frequencies 1 Hz, 35 Hz, 50 Hz and 100 Hz. Peak amplitudes have been scaled to unity.

Figure 5.9 gives the amplitude spectra of the extracted wavelets. The spectra for the wavelets modeled with $Q = 135$ are very similar. The amplitudes for these spectra slowly decay with frequency. The spectrum for the wavelet modeled with $Q = 50$ is lower in amplitude however, with lower peak frequency and a smaller bandwidth due to being more attenuated. The phase spectra in Figure 5.10 generally curve downwards from 0° before turning up to intercept the abscissa at approximately the corresponding reference frequencies from which each curve was obtained. The phase spectrum for the wavelet modeled with $Q = 50$ also starts to deviate from the general trend at frequencies higher than about 40 Hz.

Frequency bandwidths were estimated over the time window from which wavelet extractions were made for the case of no Q modeling, and for each of the modeled cases (Table 5.1). The bandwidth is the largest for no Q modeling, 133 Hz, similar for the cases modeled with $Q = 135$, about 36 Hz, and the lowest for modeling with $Q = 50$, 17 Hz. These results are reasonable as frequency bandwidth should decrease with increased attenuation. Figure 5.11 displays the frequency bandwidths of 782 ms time windows centered on the corresponding TWT, calculated over entire extraction traces. The bandwidth for the case of no Q modeling seems to be stable spanning the entire trace, while for the Q modeled traces the bandwidths gradually decrease.

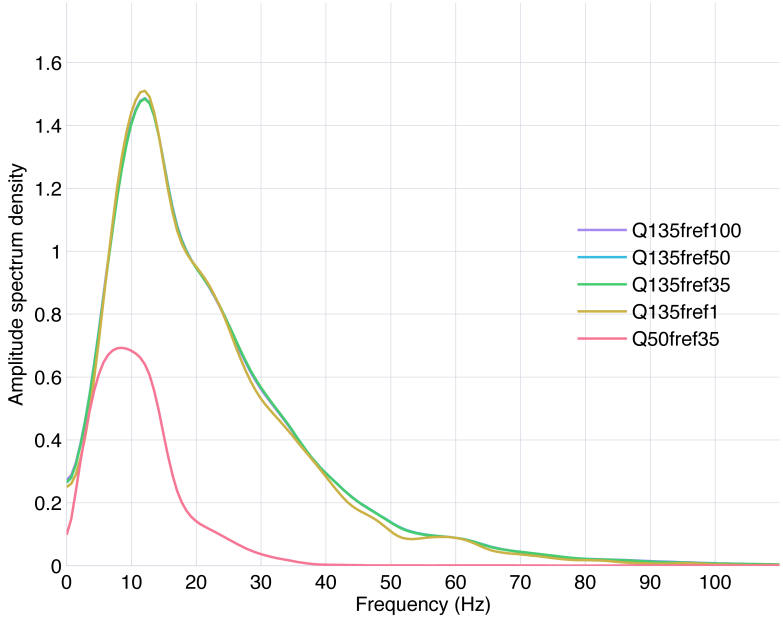

Figure 5.9: Amplitude spectra of wavelets extracted from forward Q modeled synthetic seismic with $Q = 50$ and a reference frequency of 35 Hz, and with $Q = 135$ and reference frequencies 1 Hz, 35 Hz, 50 Hz and 100 Hz.

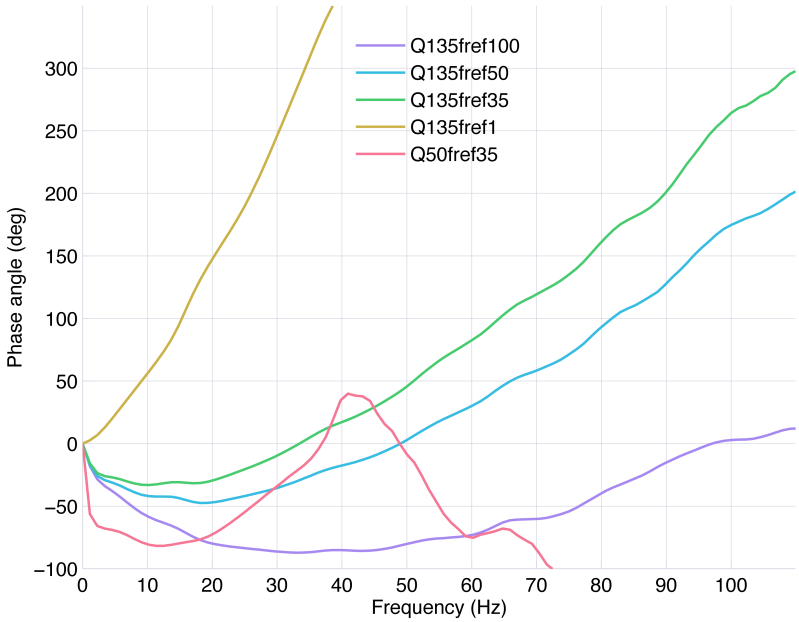

Figure 5.10: Phase spectra of wavelets extracted from forward Q modeled synthetic seismic with $Q = 50$ and a reference frequency of 35 Hz, and with $Q = 135$ and reference frequencies 1 Hz, 35 Hz, 50 Hz and 100 Hz.

Table 5.1: Bandwidths for time window between 2800-3582 ms

Case	**Bandwidth (Hz)**
No Q modeling	133.452774
$Q = 50$, $f_{ref} = 35$	17.237171
$Q = 135$, $f_{ref} = 1$	37.369320
$Q = 135$, $f_{ref} = 35$	36.912701
$Q = 135$, $f_{ref} = 50$	36.116077
$Q = 135$, $f_{ref} = 100$	35.575405

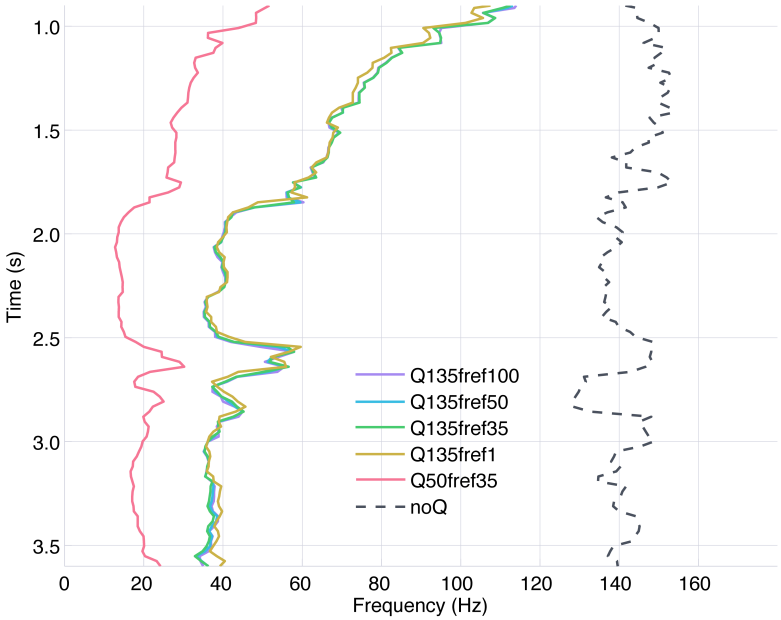

Figure 5.11: Frequency bandwidths of 782 ms time windows centered on the given TWT over traces from which wavelets were extracted, for the case of no forward Q modeling applied, forward Q modeled with $Q = 50$ and reference frequency 35 Hz, and $Q = 135$ with reference frequencies 1 Hz, 35 Hz, 50 Hz and 100 Hz. The bandwidths of the well tie time window are given at 3.19 s TWT.

6

Phase-only Q-compensation effects on a well tie at Åsgard

6.1 Experimental methods

This experiment was performed to assess the detectability of Q effects on a seismic well tie for the seismic survey MC3D-HVG2013. The time-depth relationship applied was one prepared by Statoil according to their best practice (TIME-CKS). The sampling interval of the input seismic was 4 ms, thus all data produced throughout this test were also generated with a sampling interval of 4 ms. With computational efficiency in mind, a 101x101 seismic cube was extracted from the seismic dataset surrounding well 6506/12-3, with the well positioned in the center of the cube. The cube was loaded into Matlab where phase-only forward Q modeling was performed according to to equation 3.27 (Ferber, 2005). This was done to approximately retrieve the original attenuation phase effects in the seismic prior to the phase-only Q-compensation that was applied during processing by PGS.

Starting from time zero the modeling was thus carried out with $Q = 10\,000$ for the water layer and $Q = 135$ for the sediments in the subsurface. A reference frequency of 35 Hz was used. The high Q value of 10 000 was chosen to model a non-attenuative water layer, while a Q of 135 and a reference frequency of 35 Hz was set for the sediments as these were the parameters with which the seismic survey had previously been processed. Q modeling was applied to the seismic cube using an algorithm where t* was first calculated and a filter bank gather constructed following Ferber (2005). Each filter was applied in turn to each seismic trace in the frequency domain, creating a gather of filtered traces

for each input trace. The Q modeled output traces were then calculated by interpolating between the t* values for the required time sample from each trace in a gather. This code was written by the thesis supervisor specifically for this student project.

Subsequently, the now attenuated seismic cube was phase-only Q-compensated for cases with $Q = 135$ and reference frequencies of 1 Hz, 35 Hz, 50 Hz and 100 Hz. The water layer was again modeled with $Q = 10\ 000$, while the reference frequency values were chosen with the intent of representing the range of frequencies in a typical seismic experiment. Q-compensation was applied using the same algorithm as used for forward Q modeling by switching the sign of the exponent in the filter banks with which modeling was done. Both the forward Q modeled and the Q-compensated seismic cubes were then imported into Petrel, where seismic well ties were performed for each case as well as for the original seismic survey. Well ties were first performed for a time window between 2800-3600 ms and the reflectivity series was constructed using edited sonic and density logs from well 6506/12-3.

Wavelets were extracted through ordinary coherence wavelet estimation as outlined by White (1980). A consistent set of parameters was used for all extractions, summarized in Appendix A.1, previously established by the experiment performed on synthetic data in chapter 5. The up-dip direction from the well was determined by inspecting the reflection seismic in the well area, where a general trend of very gently dipping layers was observed. This suggested that the best match location would be near the well itself. For each extraction 49 traces were scanned on either side of the well in either direction to establish the best match location. The reflectivity series was scanned with a time gate of 96 ms, thus an extracted wavelet would not be allowed to deviate more than 48 ms from the seismic.

A common trace from which to extract the wavelets was decided upon using the predictability maps produced by the software. The trace chosen was located up-dip from the well, two steps away in both the inline and crossline directions, and in an area where predictability seemed rather stable for all of the extraction cases. The optimal wavelets found for each case would therefore only differ due to the dissimilarities between the seismic cubes from which they were extracted. The wavelets were obtained with lengths of 512 ms. A second set of well ties was also performed for the shallower time window between 1600-2400 ms, to test the stability of the wavelets over time. The well ties were done with the same inputs as for the deeper time window, using an identical set of parameters and the same extraction trace. The shallower wavelets were likewise extracted with lengths of 512 ms.

All resulting wavelets were loaded into Matlab for quality control and analysis. Static time shifts were observed in both the deeper and shallower time windows of 16 ms and 12 ms, respectively, and were removed from the wavelets prior to plotting. The wavelets obtained from the modeled seismic cubes were compared against each other, first for the deeper time window and then for the shallower time window. The amplitude and phase spectra were also compared for all of the above cases. Frequency bandwidths for the deeper and shallower time windows were then estimated over the extraction traces. The bandwidths were found using a propriety software provided by Statoil based on equations 3.19 and 3.20 (Wang, 2003). For each input TWT the software calculated the corresponding frequency bandwidth over an 800 ms time window centered on the given time value. The results were plotted, and then the amplitude spectrogram for the trace from the original seismic survey was also generated in Matlab.

6.2 Results

These results test the detectability of Q phase effects on seismic well ties using a seismic survey from Åsgard. In this study a seismic cube was first phase-only forward Q modeled to approximately retrieve the attenuation phase effects present in the original seismic prior to processing. The attenuated cube was then phase-only Q-compensated for cases with $Q = 135$ and reference frequencies of 1 Hz, 35 Hz, 50 Hz and 100 Hz. Seismic well ties were performed for the forward Q modeled and the Q-compensated seismic cubes, as well as for the original seismic survey. Both a deep and a shallow time window was used, between 2800-3600 ms and 1600-2400 ms respectively. The synthetic seismograms were created from the same reflectivity series and wavelets estimated from the seismic using ordinary coherence matching (White, 1980). Predictability maps were produced by the software and used to establish a common trace over which wavelet extractions would be done in all cases. The predictability map generated for the seismic that was Q-compensated with reference frequency 35 Hz is presented as an example in Figure 6.1.

Figure 6.2 shows the wavelets obtained for the deeper time window from the modeled seismic cubes, that is for the case where no Q-compensation was applied and for cases where Q-compensation was applied with reference frequencies of 1 Hz, 35 Hz, 50 Hz and 100 Hz. The wavelet for reference frequency 1 Hz and for the seismic where no Q-compensation was applied are both delayed from time zero. The delay imposed on the latter was expected because of the earth attenuation effects modeled into the seismic. For the results from reference frequencies of 35 Hz and 50 Hz the peaks are centered

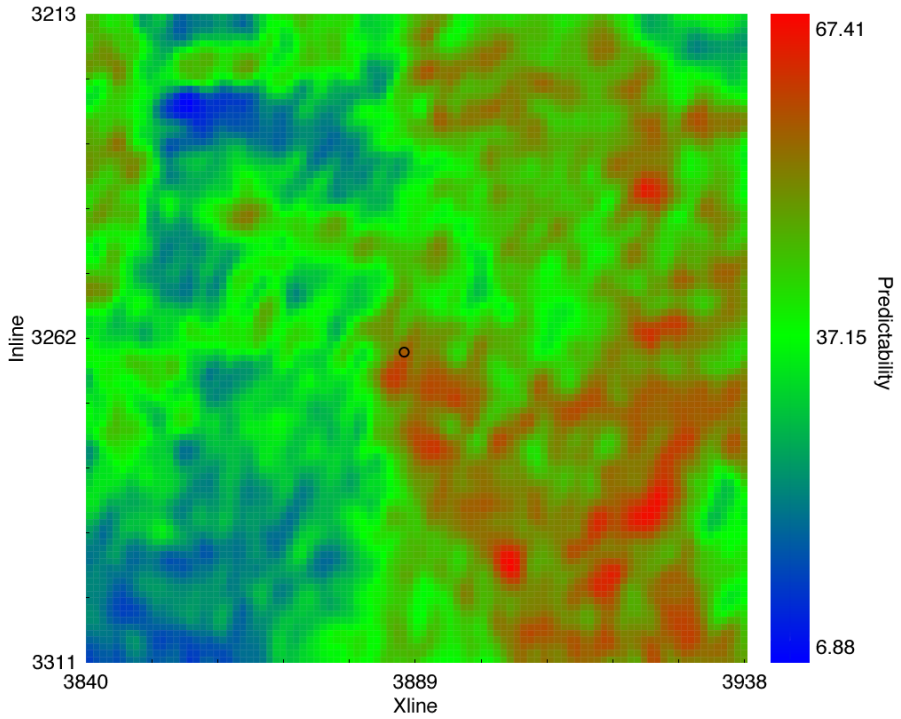

Figure 6.1: Example maximum predictability map generated for wavelet extraction from seismic Q-compensated with Q = 135 and reference frequency 35 Hz. The chosen extraction trace is marked by a black circle.

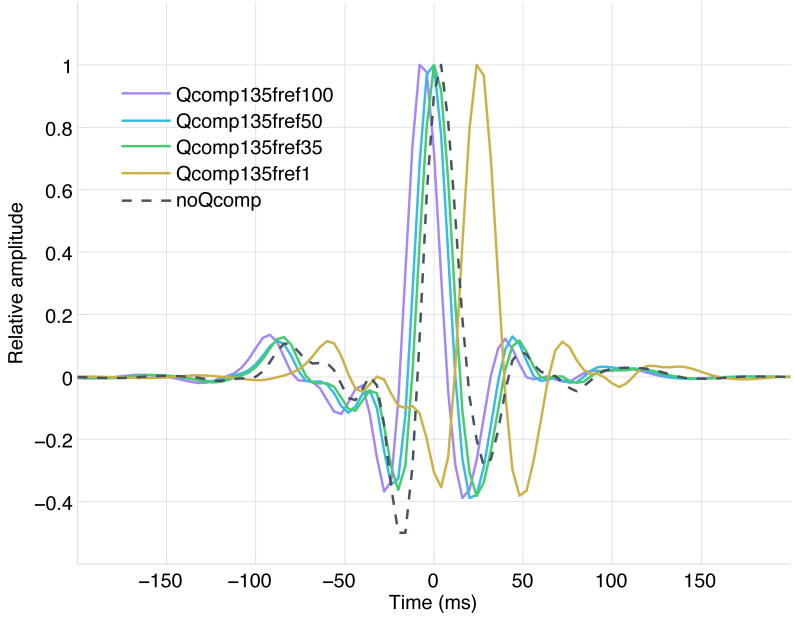

Figure 6.2: Wavelets extracted from seismic cubes in a time window between 2800-3600 ms, for the case of no Q-compensation applied and Q-compensated using Q = 135 with reference frequencies 1 Hz, 35 Hz, 50 Hz and 100 Hz. Peak amplitudes have been scaled to unity.

on time zero, however the general trend of the 50 Hz modeled wavelet seems to be leading relative to the one for 35 Hz. For reference frequency 100 Hz the wavelet is clearly leading to time zero. Thus this comparison shows that Q-compensating with sufficiently low reference frequencies will impose a delay on a wavelet, as the majority of frequency components have been forced to travel at significantly slower velocities. Likewise, Q-compensating seismic with relatively high reference frequencies will give leading wavelets, as frequency components would travel with faster velocities.

The wavelets extracted from the Q-compensated seismic are fairly symmetric, while the wavelet obtained from the seismic where no Q-compensation was applied is asymmetric. This asymmetry was also expected due to the attenuation effects in the data. Either way, Q-compensation seems to have been successful at producing wavelets with shapes expected for a typical zero phase one. The corresponding amplitude spectra are given in Figure 6.3. No significant differences in amplitude were anticipated as phase-only Q modeling was performed exclusively. Indeed the amplitude spectra are very similar for all cases, gradually decreasing towards zero at about 50 Hz.

The phase spectra in Figure 6.4 show generally rectilinear trends prior to a frequency of approximately 35 Hz. In this part of the plot, the spectrum for the case of reference frequency 1 Hz has a negative gradient, the spectra for 35 Hz and for no Q-compensation are close to zero, while the spectra for 50 Hz and 100 Hz have a positive gradient. A negative gradient thus signifies a wavelet time delay from time zero, while a positive gradient signifies an advance, which corresponds well with the observations made from Figure 6.2. Note that as the wavelet amplitudes gradually decrease towards zero, the reliabilities of the phase spectra also decrease as the phase spectra become unstable and the software experiences difficulties in interpreting them.

A comparison of the wavelets estimated from the shallower time window from the modeled seismic cubes is given in Figure 6.5, for the case where no Q-compensation was applied and for cases where Q-compensation was applied with reference frequencies of 1 Hz, 35 Hz, 50 Hz and 100 Hz. A similar trend to the one for the deeper time window is observed regarding wavelet time delay or advance from time zero, that is the wavelets are increasingly shifted earlier in time with increasing reference frequency. For this time window however, the wavelets are markedly more asymmetric. In fact, all wavelets seem to display an asymmetry typically associated with an undercorrection, that is a Q-compensation where the value used for Q was too high.

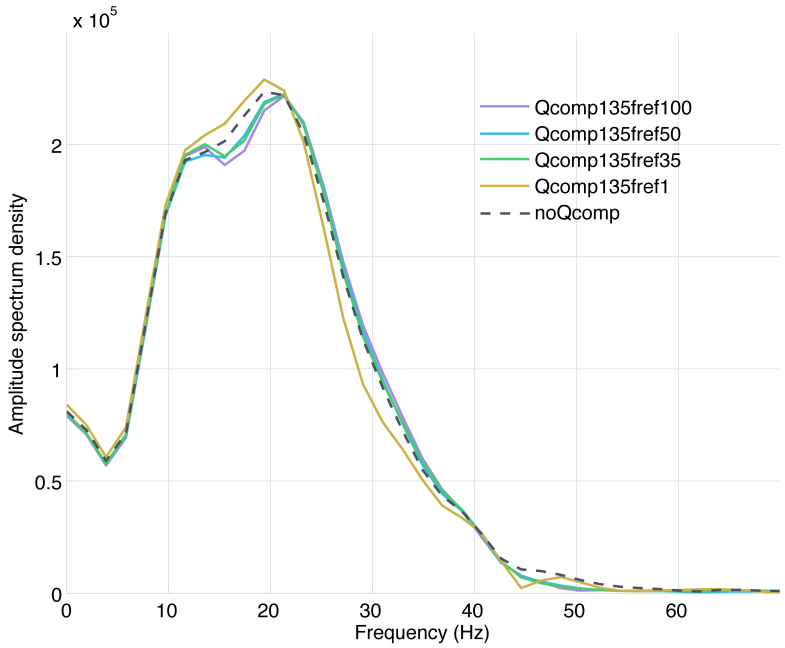

Figure 6.3: Amplitude spectra of wavelets extracted from seismic cubes in a time window between 2800-3600 ms, for the case of no Q-compensation applied and Q-compensated using Q = 135 with reference frequencies 1 Hz, 35 Hz, 50 Hz and 100 Hz.

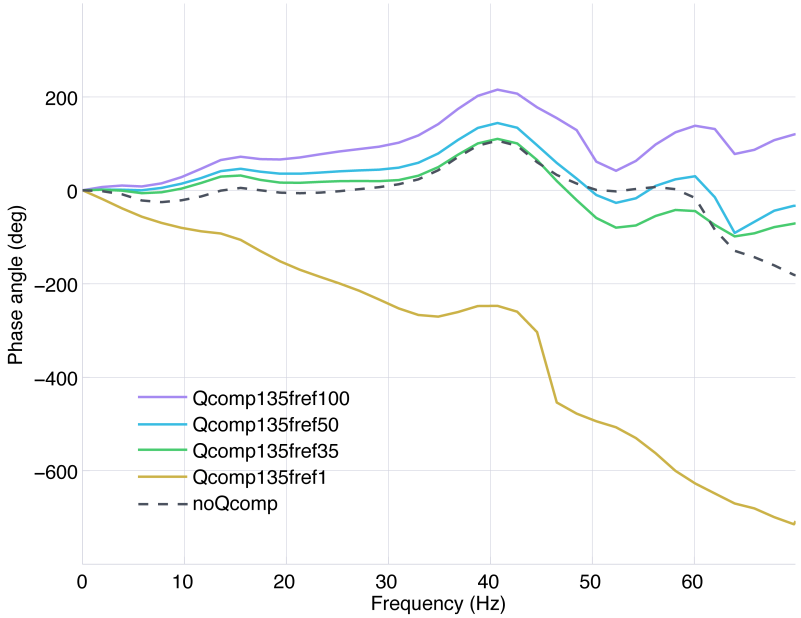

Figure 6.4: Phase spectra of wavelets extracted from seismic cubes in a time window between 2800-3600 ms, for the case of no Q-compensation applied and Q-compensated using Q = 135 with reference frequencies 1 Hz, 35 Hz, 50 Hz and 100 Hz.

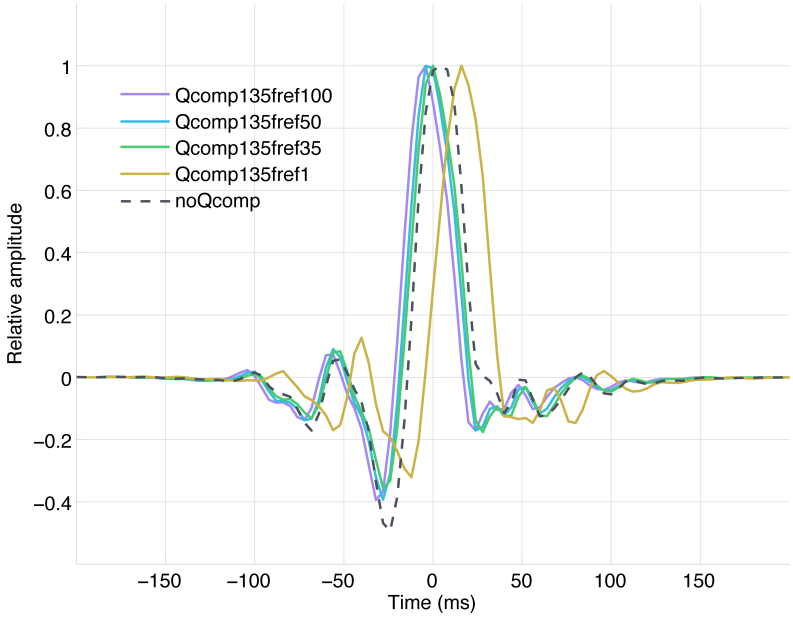

Figure 6.5: Wavelets extracted from seismic cubes in a time window between 1600-2400 ms, for the case of no Q-compensation applied and Q-compensated using Q = 135 with reference frequencies 1 Hz, 35 Hz, 50 Hz and 100 Hz. Peak amplitudes have been scaled to unity.

The amplitude spectra are also quite similar for the shallower wavelets, see Figure 6.6, decreasing steeply towards zero at around 30 Hz. The amplitude values seem to be somewhat smaller than the ones found for the deeper time window. For instance, the amplitude value of the peak frequency for the 1 Hz case is approximately 35% less than the equivalent value obtained in the deeper time window. The phase spectra of the shallower wavelets are shown in Figure 6.7. The spectra are rather rectilinear up to about 20 Hz, after which they start to deviate from the straight line pattern. Yet the trend in the lower frequency part is similar to the one observed for the wavelets from the deeper time window, where a negative gradient signifies wavelet delay from time zero and a positive gradient signifies an advance.

Frequency bandwidths were estimated for the deeper and shallower time windows over the trace from which wavelets were extracted for each of the modeled seismic cubes. The results are presented in Table 6.1. The bandwidths of the different cases are quite similar, approximately 33 Hz for the shallower time window and 25 Hz for the deeper time window. This decrease in bandwidth from the shallower to the deeper time window is reasonable as less of the higher frequency components should be present in the signal with depth. Figure 6.8 displays the frequency bandwidths of 800 ms time windows centered on the corresponding TWT, calculated over entire extraction traces.

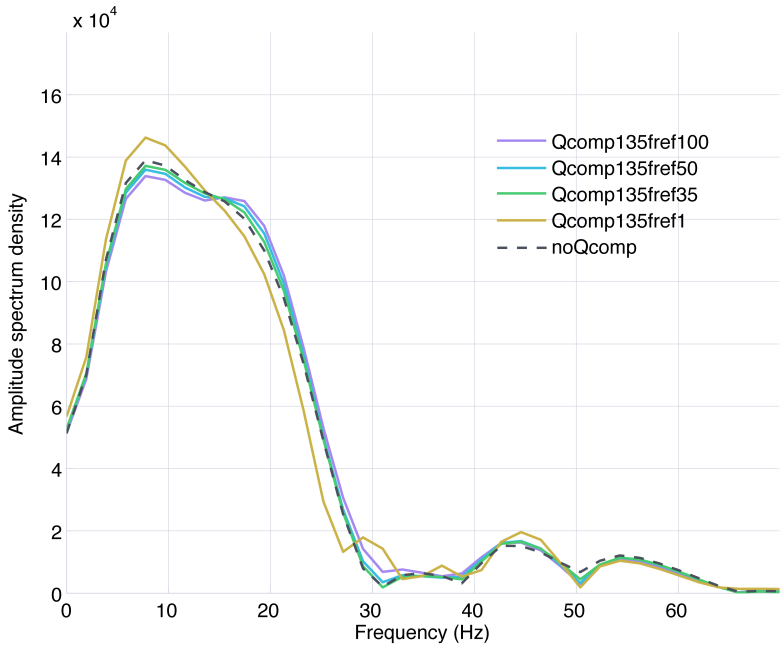

Figure 6.6: Amplitude spectra of wavelets extracted from seismic cubes in a time window between 1600-2400 ms, for the case of no Q-compensation applied and Q-compensated using Q = 135 with reference frequencies 1 Hz, 35 Hz, 50 Hz and 100 Hz.

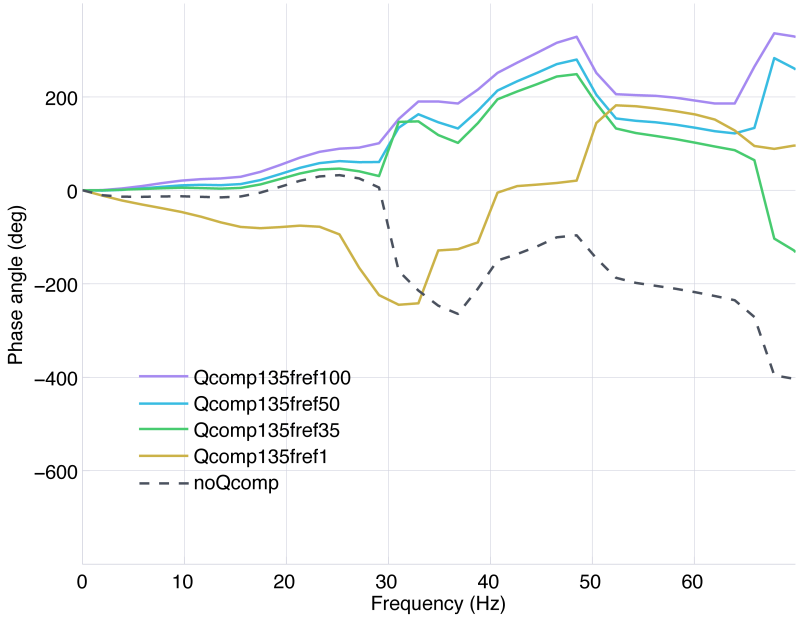

Figure 6.7: Phase spectra of wavelets extracted from seismic cubes in a time window between 1600-2400 ms, for the case of no Q-compensation applied and Q-compensated using Q = 135 with reference frequencies 1 Hz, 35 Hz, 50 Hz and 100 Hz.

Table 6.1: Bandwidths for shallow and deep time windows

Case	**Shallow bandwidth (Hz)**	**Deep bandwidth (Hz)**
Original seismic	33.005051	25.342718
No Q-compensation	33.059887	25.266600
$Q = 135$, $f_{ref} = 1$	32.671120	24.267317
$Q = 135$, $f_{ref} = 35$	33.005432	25.342993
$Q = 135$, $f_{ref} = 50$	33.069351	25.429985
$Q = 135$, $f_{ref} = 100$	33.115406	25.577667

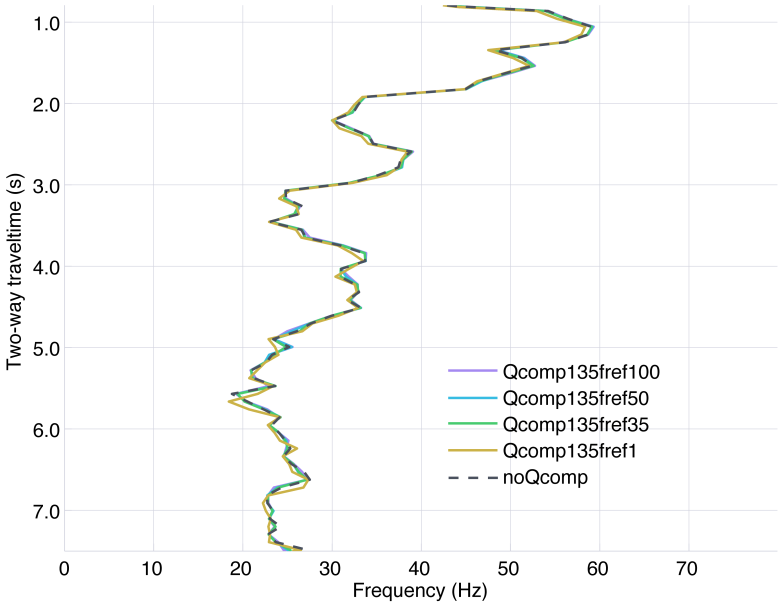

Figure 6.8: Frequency bandwidths of 800 ms time windows centered on the given TWT over traces from which wavelets were extracted, for the case of no Q-compensation applied and Q-compensated using $Q = 135$ with reference frequencies 1 Hz, 35 Hz, 50 Hz and 100 Hz. The bandwidths of the shallow and deep time windows are given at 2.0 s and 3.2 s TWT, respectively.

The amplitude spectrogram for the wavelet extraction trace from the original seismic survey is shown in Figure 6.9. It is a representation of the amplitudes associated with each frequency component in the trace at a certain time, that is the amplitude spectra at each time as viewed "from above". The spectrogram acts as a quality control for the calculated bandwidths, as the general trend of the amplitude ratios follow the trend given in Figure 6.8.

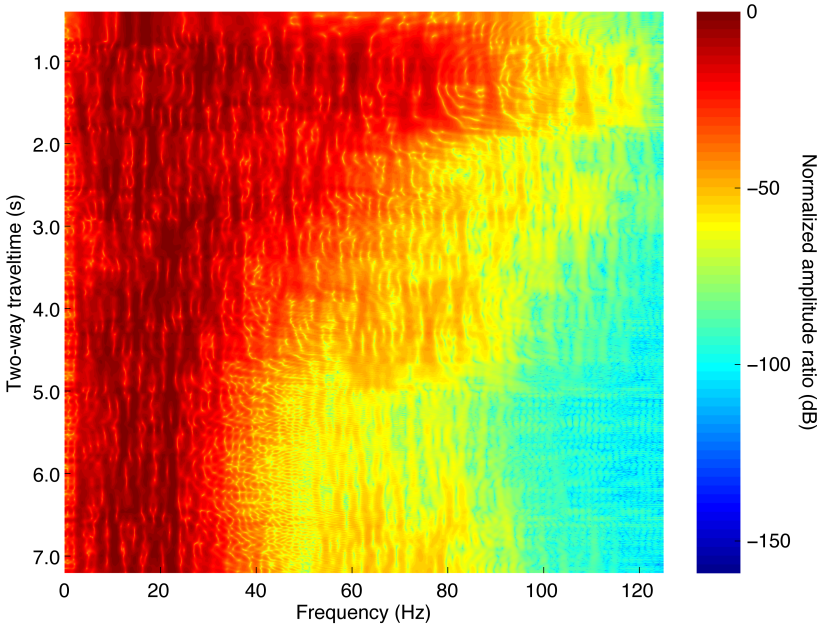

Figure 6.9: Normalized amplitude spectrogram of the wavelet extraction trace from original seismic data.

7

Discussion

The motivation for performing a controlled experiment using synthetic data was first and foremost to assess the detectability of Q effects on a seismic well tie for the best case scenario. The results show that the software successfully extracted an acceptable wavelet from seismic with a known input wavelet. The software is thus suitable for wavelet extractions. It was however noted that unreliable phase values were obtained for frequency components with sufficiently low amplitudes. Wavelets were then extracted from forward Q modeled data with results showing that the effects of Q modeling are detectable from the estimated wavelets, both with regards to modeling with different values for Q and with different values for reference frequency.

There is a connection between the time shift imposed on a wavelet, the reference frequency with which forward Q modeling was done, and the value of Q. The results show that wavelet time delay increases with reference frequency, as well as with decreasing Q. Amplitude spectra have lower peak frequencies and smaller bandwidths with decreasing Q, while the phase spectra seem to be broader and more curved for higher reference frequencies. This suggests that the outcome of imposing a time shift on such a wavelet is equivalent to a wavelet of the same shape obtained using a different reference frequency for Q modeling. Furthermore, the time shift of a wavelet might be equivalent to the time shift of a wavelet modeled with a different Q and a different reference frequency.

This experiment was performed with the very fine sampling interval of 1 ms for all data, and the input seismic was generated with a quite broad frequency bandwidth. Forward Q modeling was performed with a constant Q value for the sediments, and only one trace went into each seismic cube from which the wavelets were extracted. Furthermore,

the traces were modeled without additional complications related to internal multiples, the stacking of AVO, etc. All of these choices were made with the intent of simplifying the experiment, and with the intent of obtaining results for an ideal case. These factors limit however the application of the results to a real seismic experiment.

A second experiment was thus performed to evaluate the detectability of Q effects on a well tie using a real seismic survey. Wavelets were estimated from phase-only Q-compensated data modeled with different reference frequencies. The results show that also for this experiment the effects of Q modeling are detectable from the extracted wavelets. For the case of Q-compensation it seems that wavelet time delay increases with decreasing reference frequency, and that the slope of the phase spectra correspondingly approach and turn negative with decreasing reference frequency. Similarly this also suggests that the outcome of imposing a time shift on a wavelet is equivalent to a wavelet of the same shape obtained using a different reference frequency for Q modeling.

Seismic well ties were performed for two time windows using the same parameters, to assess the stability of the extracted wavelets with time. The most pronounced difference between the wavelets from the shallow (1600-2400 ms) and the deep (2800-3600 ms) time windows is the obvious change in shape. As the wavelets from the deeper time window seemed more or less symmetric, the wavelets from the shallower time window were clearly asymmetric. The shape of the shallow wavelets suggests that they were undercorrected. It thus seems that the constant Q value of 135 used for phase-only Q-compensation was satisfactory for the deep time window, but inappropriately high for the shallow time window. Depending on if only the shorter well tie time window is going to be applied for further analysis, or if segments of data apart from this time window likewise are going to be used, one should consider applying Q-compensation with a suitable time-variant Q function rather than with a constant Q.

Of course the validity of these results is questionable. The well ties were only performed for one well, while similar results from several wells would reinforce their reliability in application to a larger seismic region. Furthermore, wavelet extraction was done from only a single trace due to limitations imposed by the software. A suggestion would be to perform trace scanning such that wavelets from several nearby traces were combined (for instance through a weighted average) giving the best wavelet from a local area of traces. This would also serve as a way of reducing the noise involved in the matching. The number of traces scanned was somewhat low (49 traces to either side in either direction from the well), also due to software limitations. Scanning a larger region of traces would give more possibilities for the best match location.

The bandwidths of the time windows over which well ties were performed were rather low; approximately 33 Hz for the shallow window, and 25 Hz for the deep window. The uniqueness of the wavelets are uncertain especially for the deeper time window. Interestingly, the plot showing bandwidths over the entire wavelet extraction traces (Figure 6.8) indicates time windows close to the ones used with significantly higher bandwidths. It seems the windows used in this study were rather unlucky choices, bandwidth-wise. Now what if a neighbouring time window still including a target of interest actually gave a better well tie just because of the extra bandwidth? A test could be performed by moving the time window a few 100 ms to one with a higher bandwidth.

The wavelet extractions were performed with parameters estimated from the controlled experiment on synthetic data, where the sampling interval was much finer (1 ms) than for this experiment (4 ms). Perhaps a more suitable set of parameters would have been obtained for this study if the controlled experiment also had been performed using sampling intervals of 4 ms. Furthermore, phase-only Q-compensation was applied by PGS during processing to pre-stack data, while the modeling in this experiment was done on post-stack data. Thus the initial removal of the Q-compensation effects was more of an approximation rather than a true removal.

8

Conclusion

The controlled experiment using synthetic data successfully established that the software used for the seismic well ties and the wavelet extractions was suitable. Wavelets were obtained from forward Q modeled synthetic seismic that showed that Q effects were detectable from these data. A second experiment was performed using data from a real seismic survey at Åsgard. Wavelets were obtained for a deep and a shallow time window from which Q effects also were evident. The extracted wavelets were proven to be rather unstable with time, as the ones obtained for each time window differed significantly. Another effect observed was that connecting time shifts with reference frequencies and Q. Both experiments implied that the outcome of imposing a time shift on a wavelet was equivalent to a wavelet of the same shape estimated using a different reference frequency for Q modeling. The experiment on synthetic data also showed that the time shift of a wavelet might be equivalent to the time shift of a wavelet modeled with a different Q and a different reference frequency. Several assumptions were made for each of these tests, thus the validity of the results should be tested with less limitations.

9

Further work

1. Depth conversion; determine the depth error associated with the time shifts due to Q effects.
2. Establish whether method of VSP picking affects the wavelet extracted from a seismic well tie. How does the trade-off between time shift, reference frequency and Q change because of this?
3. Establish whether the stability of the wavelet extracted from a seismic well tie improves with time if a time-variant Q function is used for modeling instead of a constant Q.
4. Repeat the experiment performed in this study with seismic well ties from several wells with several extraction traces for each case.
5. Assess whether moving a well tie time window to one with higher bandwidth gives a better well tie over the target level.
6. Calculate the statistics related with wavelet extractions. What is the goodness-of-fit and accuracy of the seismic well ties?

References

Aki, K. & Richards, P. G. (2002). *Quantitative Seismology* (2nd ed.). Sausalito, CA: University Science Books.

Anstey, N. A. (1981). *Seismic Prospecting Instruments, Volume 1, Signal Characteristics and Instrument Specifications* (2nd ed.). Berlin, Germany: Gebrüder Borntraeger.

Bell, R. E., Jackson, C. A.-L., Elliott, G. M., Gawthorpe, R. L., Sharp, I. R., & Michelsen, L. (2014). Insights into the development of major rift-related unconformities from geologically constrained subsidence modelling: Halten Terrace, offshore mid Norway. *Basin Research*, *26*, 203–224. doi:10.1111/bre.12049

Bøe, R., Fossen, H., & Smelror, M. (2010). Mesozoic sediments and structures onshore Norway and in the coastal zone. *Norges geologiske undersøkelse Bulletin*, *450*, 15–32.

Czajkowski, M. K. (2014). *Putting seismic data at its true vertical depth - checkshot corrections and the interplay between attenuation/dispersion* (Unpublished student report). Department of Petroleum Engineering and Applied Geophysics, Norwegian University of Science and Technology, Norway.

Duren, R. E. & Trantham, E. C. (1997). Sensitivity of the dispersion correction to Q error. *Geophysics*, *62*(1), 288–290. doi:10.1190/1.1444129

Ferber, R. (2005). A filter bank solution to absorption simulation and compensation. In *SEG Technical Program Expanded Abstracts 2005*, (pp. 2170–2172). doi:10.1190/1.2148144

Futterman, W. I. (1962). Dispersive body waves. *Journal of Geophysical Research*, *67*(13), 5279–5291. doi:10.1029/JZ067i013p05279

Gadallah, M. R. & Fisher, R. L. (2005). *Applied seismology: a comprehensive guide to seismic theory and application.* Tulsa, OK: PennWell.

Gusmeroli, A., Clark, R. A., Murray, T., Booth, A. D., Kulessa, B., & Barrett, B. E. (2010). Seismic wave attenuation in the uppermost glacier ice of Storglaciären, Sweden. *Journal of Glaciology*, *56*(196), 249–256. doi:10.3189/002214310791968485

Jensen et al. (1985). *Completion Report, 6506/12-3.* Retrieved 10/06/2015 from factpages.npd.no

Koch, J.-O. & Heum, O. R. (1995). Exploration trends of the Halten Terrace. In Hanslien, S. (Ed.), *Petroleum Exploration and Exploitation in Norway*, volume 4 of *Norwegian Petroleum Society Special Publications*, (pp. 235–251). doi:10.1016/S0928-8937(06)80044-5

Kreyszig, E. (2006). *Advanced engineering mathematics* (9th ed.). Hoboken, NJ: Wiley.

Martinius, A. W., Ringrose, P. S., Brostrøm, C., Elfenbein, C., Næss, A., & Ringås, J. E. (2005). Reservoir challenges of heterolithic tidal sandstone reservoirs in the Halten Terrace, mid-Norway. *Petroleum Geoscience*, *11*, 3–16. doi:10.1144/1354-079304-629

Percival, D. B. & Walden, A. T. (1993). *Spectral analysis for physical applications: multitaper and conventional univariate techniques.* Cambridge, England: Cambridge University Press.

Sheriff, R. E. & Geldart, L. P. (1995). *Exploration Seismology* (2nd ed.). Cambridge, England: Cambridge University Press.

Simm, R. & Bacon, M. (2014). *Seismic Amplitude: An Interpreter's Handbook.* Cambridge, England: Cambridge University Press.

Simm, R. & White, R. E. (2002). Tutorial: Phase, polarity and the interpreter's wavelet. *First Break*, *20*(5), 277–281.

Urbanek, L.-E. (2014). *Data Processing Report, MC3D-HVG2013.* Internal Statoil report.

Walden, A. T. & White, R. E. (1984). On errors of fit and accuracy in matching synthetic seismograms and seismic traces. *Geophysical Prospecting*, *32*(5), 871–891. doi:10.1111/j.1365-2478.1984.tb00744.x

Walden, A. T. & White, R. E. (1998). Seismic wavelet estimation: a frequency domain solution to a geophysical noisy input-output problem. *IEEE Transactions on Geoscience and Remote Sensing*, *36*, 287–297. doi:10.1109/36.655337

Wang, Y. (2003). Quantifying the effectiveness of stabilized inverse Q filtering. *Geophysics*, *68*, 337–345. doi:10.1190/1.1543219

Wang, Y. (2008). *Seismic Inverse Q Filtering.* Oxford, England: Blackwell.

White, R. E. (1980). Partial coherence matching of synthetic seismograms with seismic traces. *Geophysical Prospecting*, *28*(3), 333–358. doi:10.1111/j.1365-2478.1980.tb01230.x

White, R. E. (1997). The accuracy of well ties: Practical procedures and examples. In *SEG Technical Program Expanded Abstracts 1997*, (pp. 816–819). doi:10.1190/1.1886137

White, R. E. & Simm, R. (2003a). Tutorial: Good practice in well ties. *First Break*, *21*(10), 75–83.

White, R. E. & Simm, R. (2003b). The Importance of Bandwidth in Seismic Cross Equalisation – Well Tie and Other Examples. In *EAGE 65th Conference and Exhibition*, Extended Abstract P071.

White, R. E., Thomas, R. T., & Castoro, A. (1998). Stretch and Squeeze - Just Keeping up Appearances? In *EAGE 60th Conference and Exhibition*, Extended Abstract P138. doi:10.3997/2214-4609.201408412

Zaki et al. (2011). *Åsgard Reservoir Management Plan.* Internal Statoil document.

Appendix

A.1 Parameters used for wavelet extractions

In this study seismic well ties were performed in Petrel 2014.5, where wavelets were extracted using the *Deterministic* method and the *Extended White* algorithm. The well ties were done for well 6506/12-3 with a time-depth relationship prepared by Statoil according to their best practice (TIME-CKS). Synthetic seismic cubes and cubes modeled from seismic survey MC3D-HVG2013 were input, while reflection coefficients were calculated from edited sonic velocity and density logs. Values that were chosen for specific parameters are summarized in Table A.1. Default values were applied otherwise.

Table A.1: Parameters used for ordinary coherence wavelet extractions

Parameter	**Synthetic seismic**	**Real seismic**
Inline	3262	3264
Xline	3889	3887
Inline window	1	49
Xline window	1	49
Length of extraction xcorr	256 ms	256 ms
RC window		
Start (a)	2800 ms	1600/2800 ms
Length (b)	782 ms	800/800 ms
RC window scan		
Offset to center (d)	0 ms	0 ms
Length (e)	40 ms	96 ms